Cell Reports

Article

Multi-site investigation of gut microbiota in CDKL5 deficiency disorder mouse models: Targeting dysbiosis to improve neurological outcomes

Graphical abstract

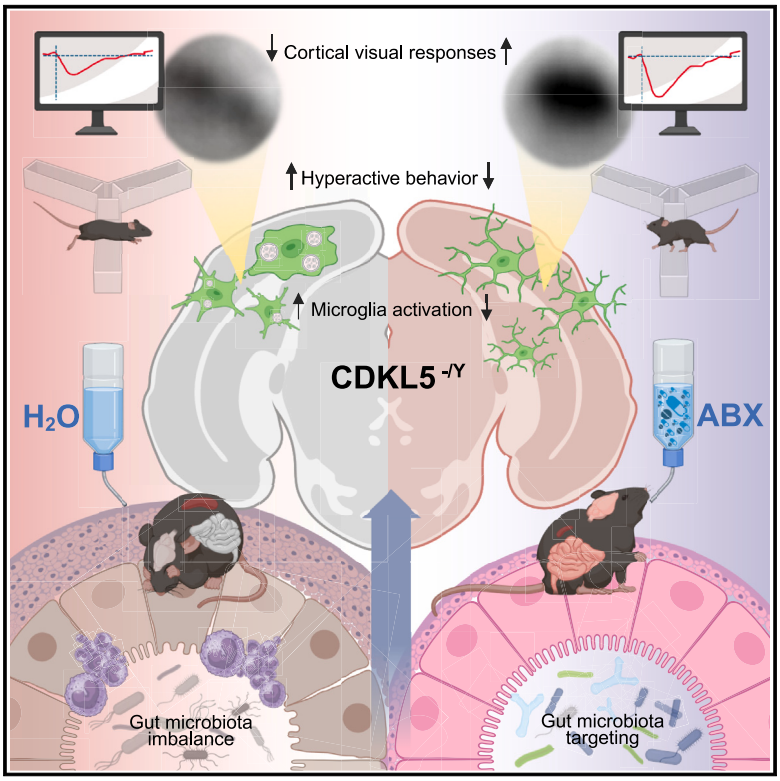

Highlights

- The gut microbiota composition in CDD mice differs from that of WT mice
- Antibiotic treatment counteracts dysbiosis, improving behavior and neuronal responses
- Fecal transplantation transfers the phenotype from CDKL5 KO mice to WT recipients
- Targeting the gut microbiota could be a therapeutic strategy for CDD patients

Authors

Francesca Damiani, Maria Grazia Giuliano, Sara Cornuti, ..., Vera M. Kalscheuer, Tommaso Pizzorusso, Paola Tognini

Correspondence

paola.tognini@santannapisa.it

In brief

Damiani et al. show that CDKL5 deficiency disorder mouse models have an altered gut microbiota composition. Targeting intestinal microbes through antibiotics improves behavior, visual responses, and microglia phenotype. Finally, a causal link between the CDKL5 KO microbiota and the observed phenotype is demonstrated through fecal transplantation into WT recipient mice.

Damiani et al., 2025, Cell Reports *44*, 115546
April 22, 2025
https://doi.org/10.1016/j.celrep.2025.115546

CellPress

Cell Reports

CellPress
OPEN ACCESS

Article

Multi-site investigation of gut microbiota in CDKL5 deficiency disorder mouse models: Targeting dysbiosis to improve neurological outcomes

Francesca Damiani,[1] Maria Grazia Giuliano,[1,2] Sara Cornuti,[1] Elena Putignano,[3] Andrea Tognozzi,[1,4] Vanessa Suckow,[5] Vera M. Kalscheuer,[5] Tommaso Pizzorusso,[1,3] and Paola Tognini[2,6,*]

[1]Laboratory of Biology BIO@SNS, Scuola Normale Superiore, Piazza dei Cavalieri 7, 56126 Pisa, Italy
[2]Health Science Interdisciplinary Center, Sant'Anna School of Advanced Studies, Piazza Martiri della Libertà 33, 56127 Pisa, Italy
[3]Institute of Neuroscience, National Research Council, Via G. Moruzzi 1, 56124 Pisa, Italy
[4]PhD Program in Clinical and Translational Science, University of Pisa, Via Savi 10, 56126 Pisa, Italy
[5]Max Planck Institute for Molecular Genetics, Ihnestraße 63, 14195 Berlin, Germany
[6]Lead contact
*Correspondence: paola.tognini@santannapisa.it
https://doi.org/10.1016/j.celrep.2025.115546

SUMMARY

Cyclin-dependent kinase-like 5 (CDKL5) deficiency disorder (CDD) is a rare neurodevelopmental disorder often associated with gastrointestinal (GI) issues and subclinical immune dysregulation, suggesting a link to the gut microbiota. We analyze the fecal microbiota composition in two CDKL5 knockout (KO) mouse models at postnatal days (P) 25, 32 (youth), and 70 (adulthood), revealing significant microbial imbalances, particularly during juvenile stages. To investigate the role of the intestinal microbiota in CDD and assess causality, we administer antibiotics, which lead to improved visual cortical responses and reduce hyperactivity. Additionally, microglia morphology changes, indicative of altered surveillance and activation states, are reversed. Strikingly, fecal transplantation from CDKL5 KO to wild-type (WT) recipient mice successfully transfers both visual response deficits and hyperactive behavior. These findings show that gut microbiota alterations contribute to the severity of neurological symptoms in CDD, shedding light on the interplay between microbiota, microglia, and neurodevelopmental outcomes.

INTRODUCTION

Cyclin-dependent kinase-like 5 (CDKL5) deficiency disorder (CDD) is an X-linked early-onset encephalopathy caused by mutations in the CDKL5 gene. The estimated prevalence of this condition is 1 in 40,000 to 1 in 60,000 live births. Patients with CDD exhibit severe global developmental delays, including early-onset epileptic encephalopathy, intellectual disability, visual and motor impairments, strong hypotonia, sleep disturbances, and hand stereotypies.[1–3] Some of these symptoms overlap with Rett syndrome (RTT); however, the key distinctions include the absence of a regression period and the early onset of seizures in patients with CDD. Currently, there are no available treatments for CDD.

A common issue in patients with CDD is the presence of gastrointestinal (GI) problems, including diarrhea, constipation, and acidic reflux.[4] This may be linked to subclinical immune dysregulation, likely stemming from a faulty inflammation regulatory signaling system.[5,6] Remarkably, GI disorders are about four times more common in children with autism spectrum disorders (ASD) than in neurotypical children.[7] Also, other central nervous system (CNS)-related comorbidities, such as seizures and sleep disorders, tend to occur more frequently in individuals with GI dysfunction in the ASD population.[8–10] The heightened occurrence of GI dysfunction in ASD, coupled with its substantial correlation with challenging behaviors and psychiatric comorbidities, suggests a possible link between gut and brain dysfunction in neurodevelopmental disorders such as CDD. At least part of this association could be due to abnormal composition of the gut microbiome (i.e., the ecosystem of microorganisms residing in the GI tract that engage symbiotic interactions with their host).[11,12] Indeed, patients with ASD display alterations in the composition of the gut microbiota[13] as well as patients with RTT.[14,15] Importantly, we have recently discovered differences in biodiversity and composition of intestinal microbes in a cohort of Italian patients affected by CDD.[16] Disturbances in the composition or equilibrium of the gut microbiota, termed dysbiosis, have been associated with inflammatory bowel disease (IBD), metabolic disturbances, and even neuropsychiatric conditions.[17–20] Nevertheless, the composition of the intestinal microbiota in widely used CDD models and the impact of alterations in microbiota composition on neurologically relevant outcomes have not been explored.

To investigate the link between CDD symptoms and the gut-brain axis, we analyzed the developmental trajectory of the fecal microbiota in CDKL5 mouse models at distinct ages, and found

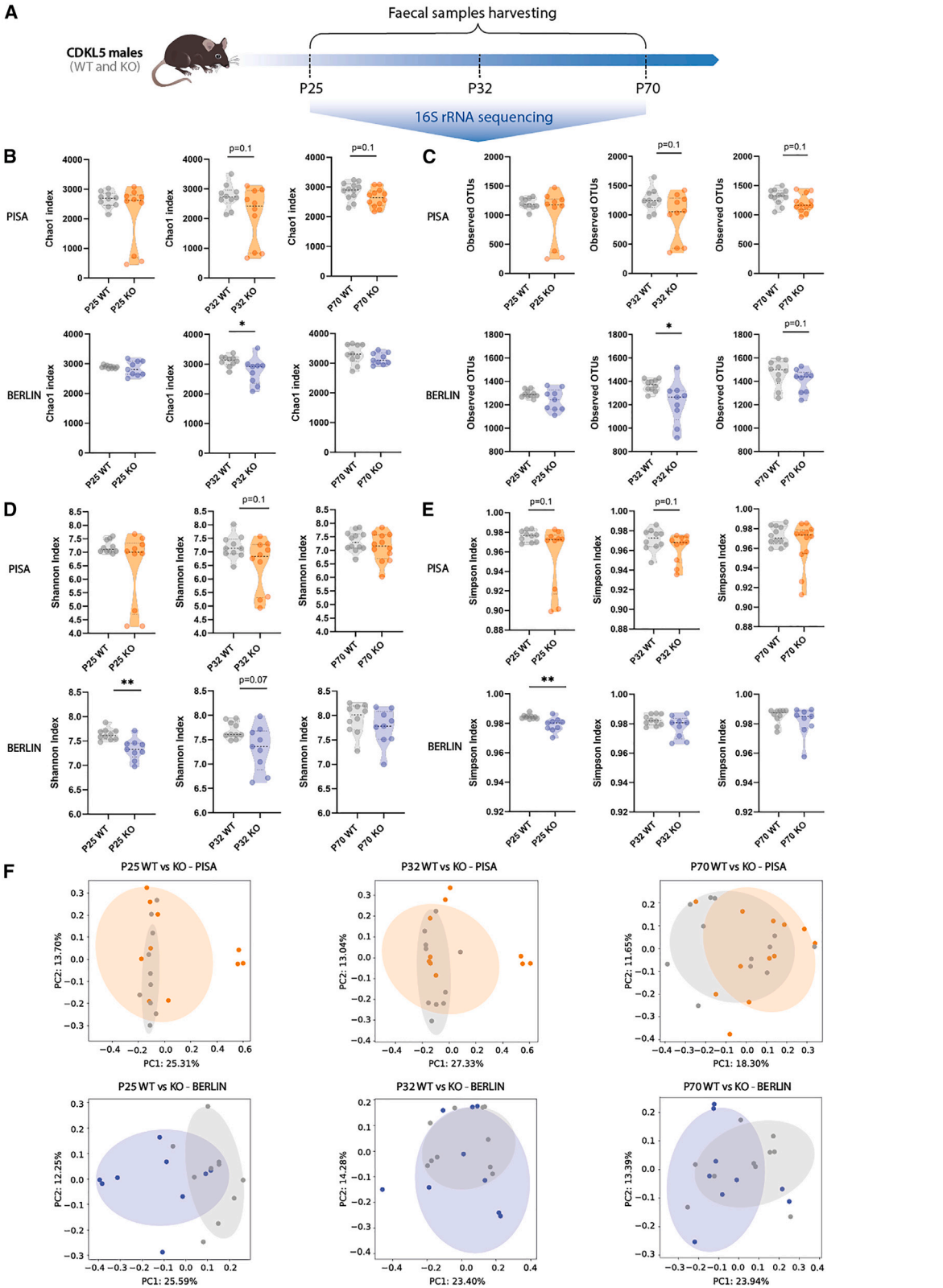

(legend on next page)

significant differences compared to wild-type (WT) littermates. Since the intestinal microbiota is strongly affected by environmental factors, our investigation was performed considering two CDKL5 null mouse models living in different facilities in Italy and Germany. Our findings unveiled the presence of a potential gut microbiota composition imbalance, suggesting a negative impact of the intestinal microbes of CDKL5 mutants on neurological outcomes. To test this hypothesis, we targeted the gut microbiota by a 25-day treatment with an antibiotic cocktail (ABX) and we assessed visual cortical responses and behavioral performance. Moreover, we analyzed microglia alterations as a possible cellular underpinning of the ABX effect. The results revealed that ABX intervention partially rescued this phenotype, indicating an improvement in the potential inflammatory state of the brain in CDD. Finally, fecal microbiota transplantation from CDKL5 KO to WT recipient mice transferred the neurological impairments of the CDD mouse model. Overall, our study shows that microbial manipulation could be a novel and non-invasive strategy to improve symptoms in patients with CDD.

RESULTS

Alterations in the composition of CDKL5 KO fecal microbiota

To investigate the composition of intestinal bacteria, fresh fecal samples were collected longitudinally from both CDKL5 KO and WT mice. Sampling occurred longitudinally at postnatal day 25 (P25), again at P32, and during adulthood at P70 (see Figure 1A). Bacterial DNA was then extracted from these fecal samples and subjected to analysis using 16S rRNA sequencing (rRNA-seq).

Given that the composition of gut microbiota can be influenced by environmental factors, including the animal's living conditions (i.e., the vivarium), we conducted our analysis on two different CDKL5 null mouse lines born and raised in two distinct animal facilities: the vivarium at the National Research Council in Pisa, Italy, and the vivarium at the Max Planck Institute for Molecular Genetics in Berlin, Germany. This parallel analysis of CDD mouse models from different facilities served to increase the robustness of the differences observed in our experiments.

Bacterial relative abundance is reported in Table S1 (Pisa vivarium) and Table S2 (Berlin vivarium).

To analyze the results, we first calculated alpha diversity, a parameter reflecting species richness or evenness in a microbial ecosystem.[21] A high alpha diversity is generally associated with a healthy microbiome condition, while a reduction has been observed in a variety of diseases such as obesity,[22] colitis, IBD,[23] and to some extent neurological disorders.[24] We calculated four different indexes and found a significant decrease in the Chao1 index (Figure 1B) and observed operational taxonomic unit (OTU) (Figure 1C) at P32 in the CDKL5 KO mice raised in the Berlin vivarium. This result was paralleled by a tendency toward a significant decrease in alpha diversity in the CDKL5 KO mice from Pisa vivarium (Figures 1B and 1C). Moreover, Shannon index and Simpson index were decreased in the CDKL5 KO mice at P25 with respect to WT littermates in the Berlin vivarium (Figures 1D and 1E).

Second, we computed beta diversity, which measures the degree of phylogenetic similarity between microbial communities, using the Bray-Curtis dissimilarity.[25] The principal coordinates analysis (PCoA) of the distance matrix of the fecal microbiota belonging to all the animals raised in the Pisa vivarium with respect to the ones raised in Berlin showed, as expected, a distinct clustering of the samples (Figure S1). PCoA at the three different ages demonstrated the presence of a certain degree of clustering of fecal microbiota in WT animals versus CDKL5 KO mice. Specifically, significant phylogenetic dissimilarities were present between CDKL5 KO mice and WT littermates at P32 in the Pisa vivarium and at P25 in the Berlin vivarium (Figure 1F).

Third, we sought to explore differences in the bacterial composition between juvenile and adult WT and CDKL5 KO mice by using the linear discriminant analysis (LDA) effect size (LEfSe) method.[26] LEfSe analysis revealed taxonomic dissimilarities between WT and CDKL5 KO mice in both the Pisa and Berlin facilities (Figures 2A–2E). In the Pisa vivarium, such differences were more pronounced during juvenile ages (P25 and P32, Figures 2A and 2B) with respect to P70 (Figure 2C; see also Figure S2). In particular, the family Alcaligenaceae and the orders Burkholderiales and Pasteurellales were enriched in the CDKL5 KO microbiota at both P25 and P32. Together with Enterobacteriaceae and Epsilonproteobacteria enriched only in the P25 CDKL5 KO microbiota (Figure 2A), those taxa belong to the phylum Proteobacteria. Emerging evidence identified the Proteobacteria (or Pseudomonadota) phylum as a possible microbial signature of disease.[27,28] Notably, the family Bacteroidaceae were significantly enriched in the fecal microbiota of CDKL5 KO mice with respect to WT littermates at all ages (Figures 2A–2C). In the Berlin facility, the cladogram displayed a significant enrichment of the family Porphyromodanaceae, Prevotellaceae, and Lactobacillaceae, in the class Bacteroidia, in the order Sphingobacteriales, and again in the family Bacteroidaceae in the P25 CDKL5 KO

Figure 1. Longitudinal characterization of the gut microbiota in CDKL5 KO mice raised in Pisa or Berlin vivaria

(A) Experimental timeline. Mice were single housed starting from weaning onward, and fecal samples were collected at postnatal day (P)25, P32, and P70 (n = 9–12 animals/group).

(B–E) Violin plots showing alpha diversity comparison between WT and KO mice from Pisa (top plots) and Berlin (bottom plots) vivaria: (B) CHAO1 index, (C) observed OTUs, (D) Shannon index, (E) Simpson index. Each dot represents a single animal. Median alpha diversity is shown as black dotted horizontal line (n = 9–12 mice/group, Mann-Whitney U test, *$p \leq 0.05$, **$p < 0.01$).

(F) PCoA plot based on Bray-Curtis dissimilarity matrix showing beta diversity of WT and KO mice from Pisa (top plots) and Berlin (bottom plots) vivaria. The ellipses represent 95% confidence intervals for each group. Axes in the PCoA display the percentage of variation explained using Bray-Curtis dissimilarity (Permutational Multivariate Analysis of Variance [PERMANOVA]) test; mice from PISA, P25 KO versus P25 WT pseudo-F = 1.718 p = 0.058, P32 KO versus P32 WT pseudo-F = 1.839 p = 0.038, P70 KO versus P70 WT pseudo-F = 1.421 p = 0.097; mice from BERLIN, P25 KO versus P25 WT pseudo-F = 1.817 p = 0.002, P32 KO versus P32 WT pseudo-F = 1.060 p = 0.345, P70 KO versus P70 WT pseudo-F = 1.053 p = 0.332).

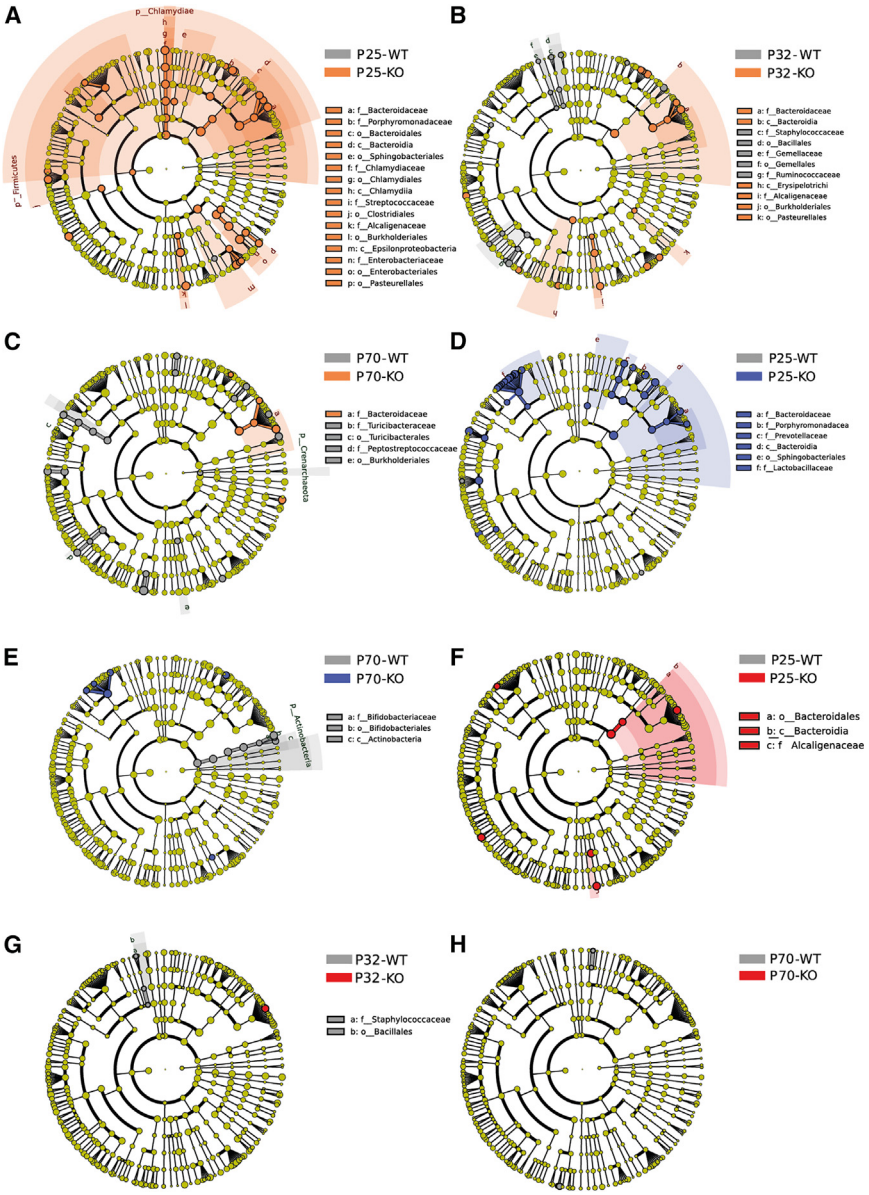

Figure 2. LDA of effect size of the fecal microbiota in WT vs. CDKL5 KO mice

Taxonomic cladograms resulted from LEfSe analysis, showing significantly differentially enriched taxa (relative abundance $\geq$0.5%) for taxonomy level L7 (species) between WT and KO mice, at different ages, in Pisa and Berlin facilities. The colors represent the genotype in which the indicated taxa is more abundant with respect to the other genotype. Differential taxa were determined based on an LDA threshold score of >2.5.

(A–C) Taxonomic differences between WT and KO mice from the Pisa vivarium, at P25 (A), P32 (B), and P70 (C).

(D and E) Taxonomic differences between WT and KO mice from the Berlin vivarium, at P25 (D) and P70 (E). No differences were observed at P32 for the mice living in the Berlin facility.

(F–H) LEfSe of the fecal microbiota in WT vs. KO mice subtracting the variable mouse facility at P25 (F), P32 (G), and P70 (H).

mouse vs. WT littermates (Figure 2D), suggesting that the family Bacteroidaceae is a potential signature of the CDD mouse gut microbiota. While at P32 the LEfSe showed no differences, at P70 WT mice showed an enrichment of taxa related to intestinal health and probiotics, such as Bifidobacteriaceae, with respect to CDKL5 KO mice (Figure 2E). Notably, *Bifidobacterium longum*, considered a probiotic species, was significantly decreased at P70 in both the Pisa and Berlin CDKL5 KO mice (Figures 2C–2E).

To further explore the taxa alteration signature of CDKL5 KO vs. WT littermate gut microbiota, we subtracted the variable "vivarium" in the LEfSe analysis, grouping together WT and CDKL5 KO mice from Pisa and Berlin. At P25, CDKL5 KO mice displayed a significant enrichment in taxa belonging to the order Burkholderiales, family Alcaligenaceae, and in Bacteroidales. The genera *Sutterella*, *Lactobacillus*, and *Ruminococcus* were also taxa characterizing the CDKL5 KO microbiota (Figures 2F and S3). At both P25 and P32, *Bacteroides rodentium*, belonging to the family Bacteroidaceae, was enriched in the CDKL5 KO microbiota (Figures 2G and S3). Finally, the microbiota of CDD mice seem to be defective in the genera *Allobaculum* and *Parapedobacter* at P70 compared to WT littermates (Figures 2H and S3).

Although, as expected, the differences between CDKL5 KO and WT mice in the Pisa and Berlin vivarium did not perfectly overlap, our analysis highlighted significant changes in specific signature taxa in both mouse facilities, pointing toward stronger differences at younger ages.

Overall, our findings provide valuable insights into the dynamic relationship between gut microbiota composition and CDKL5 deficiency, shedding light on potential microbial signatures associated with this disorder across different developmental stages and environmental settings.

Given the prevalent differences in gut microbiota composition during juvenile stages, we decided to investigate potential alterations in intestinal structure and function in young mice from the Pisa vivarium (Figure 3A). No significant differences were detected in fecal water content at P25, P32, and P42 (Figure 3B). Similarly, no changes were observed in defecation frequency (Figure 3C), gastric transit time (Figure 3D), total GI length (Figure 3E), or colon length (Figure 3F) between CDKL5 KO and WT littermates.

Despite the absence of functional differences, we observed a significant increase in the gene expression of trefoil factor 3 (*Tff3*), zonula occludens 1 (tight junction protein 1 *Tjp1*), and

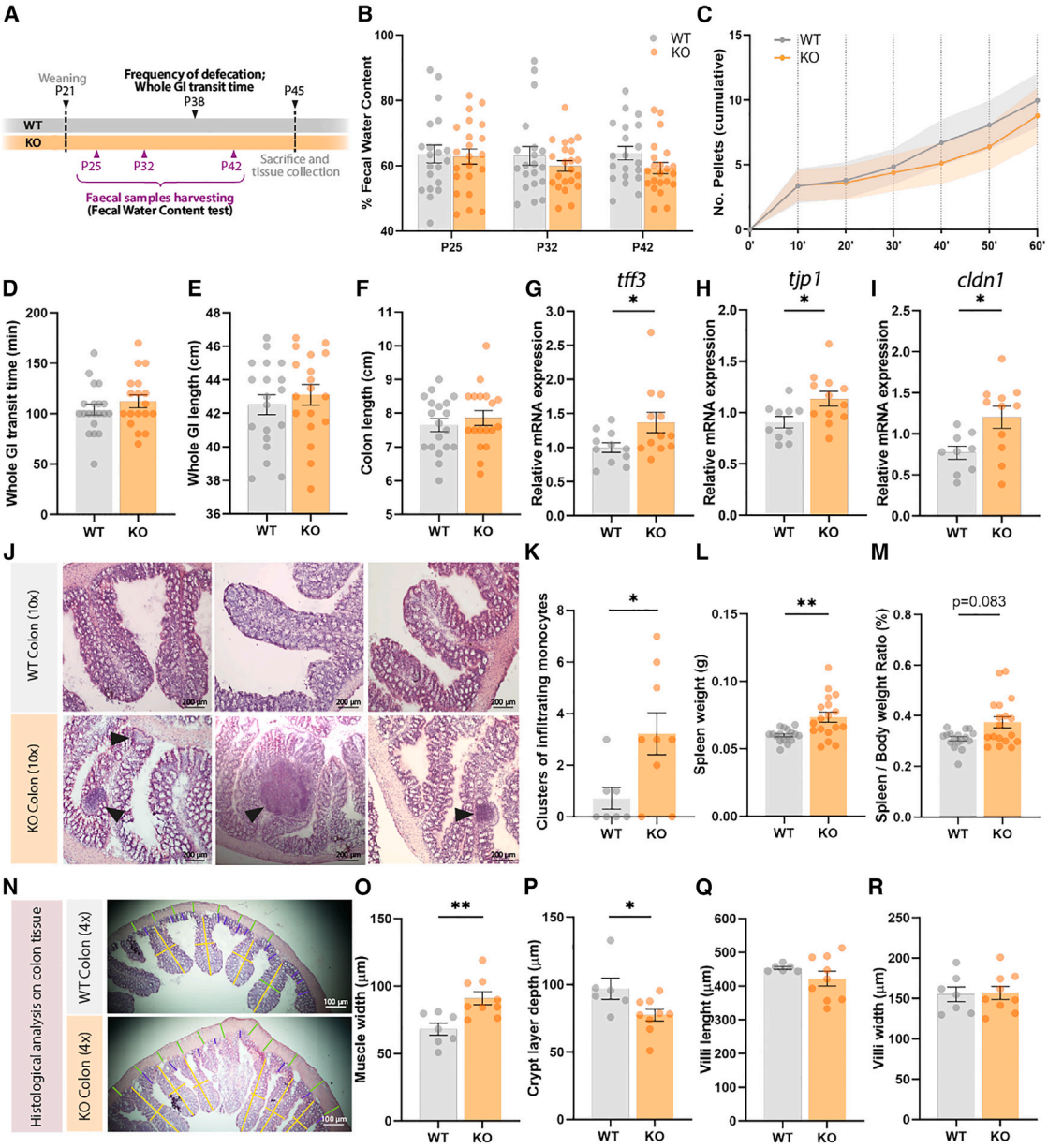

Figure 3. Gut microbiota imbalance in CDKL5 KO mice is associated with altered gut anatomy, intestinal barrier gene expression, and spleen size, with no clear signs of gastrointestinal motility defects

(A) Experimental timeline. Mice were individually housed from weaning (P21) onward. Functional tests were conducted to evaluate potential differences in GI motility.

(B–D) Evaluation of GI function (n = 18–22 mice/group). (B) % of fecal water content evaluated at P25, P32, and P42 (P25 WT vs. P25 KO unpaired t test $p = 0.696$; P32 WT vs. P32 KO Mann-Whitney U test $p = 0.675$; P42 WT vs. P42 KO Mann-Whitney U test $p = 0.110$). (C) Cumulative distribution of the number of pellets expelled over a 1-h period, with counts taken every 10 min (two-sample Kolmogorov-Smirnov test, D = 0.285, $p = 0.962$). (D) Whole GI transit time obtained by oral administration of Evan's Blue solution (unpaired t test $p = 0.323$).

(E and F) (E) Whole GI length of WT versus KO mice (unpaired t test $p = 0.489$) and (F) colon length of WT versus KO mice (unpaired t test $p = 0.465$).

(G–I) Relative mRNA expression of *tff3*, *tjp1*, *cldn1* (n = 11–12 mice/group, *tff3* Mann-Whitney U test $^*p = 0.043$, *tjp1* unpaired t test $^*p = 0.023$, *cldn1* unpaired t test $^*p = 0.018$).

(J) Representative histological colon sections of three WT (top row) and three KO (bottom row) mice showing evident monocytic infiltration in the KO mice (magnification 10×; scale bar, 200μm; black arrows show clusters of infiltrating monocytes).

(K) Number of clusters of infiltrating monocytes (Mann-Whitney U test $^*p = 0.041$).

(L) Absolute spleen weight (g) (unpaired t test $^{**}p = 0.001$).

(M) Spleen-to-body weight ratio (%) (Mann-Whitney U test $p = 0.083$).

(legend continued on next page)

claudin 1 (*Cldn1*) in the colon of CDKL5 KO mice compared to WT mice (Figures 3G–3I). These findings align with the increased monocyte infiltration observed in the colon of CDKL5 KO mice (Figures 3J and 3K), suggesting a compensatory upregulation of tight junction components to protect the intestinal epithelium and preserve barrier integrity during inflammation.[29,30] Additionally, CDKL5 KO animals exhibited an increase in spleen weight compared to WT (Figures 3L and 3M), which may reflect the presence of systemic inflammation. Finally, structural analysis of the colon (Figure 3N) revealed a significant increase in muscle layer width (Figure 3O) and a decrease in crypt layer depth (Figure 3P) in CDKL5 KO compared to WT animals, while no alterations were observed in villi length or width (Figures 3Q and 3R). These findings suggest potential remodeling of the intestinal architecture in CDKL5 KO mice, possibly as an adaptive response to inflammation or altered gut homeostasis.

Antibiotic treatment improves functional and behavioral outcomes in CDKL5 KO mice

As the composition analysis revealed differences in the CDKL5 fecal microbiota, we hypothesize the presence of a gut microbial imbalance condition. Dysbiosis has been observed in several neuropsychiatric disorders[31] and, in mouse models, has been linked to behavioral and brain functional impairments.[11,32] Therefore, we treated the Pisa vivarium mice with an antibiotic cocktail (ABX) in drinking water to target intestinal microbes, particularly bacteria taxa, and tested the potential improvement in functional and behavioral outcomes. As prominent differences in the fecal microbiota were observed in the CDKL5 null mouse at younger ages in both the Pisa and Berlin facilities, mice were subjected to ABX administration from weaning (P21) for the next 24 days (Figure 4A).

As the gut bacteria are involved in energy harvesting from the ingested food, we monitored the body weight of the treated mice. We observed a slight but significant reduction in body weight in ABX-treated CDKL5 KO mice compared to CDKL5 controls (CTRL, drinking regular water) at P28, with a similar trend at P34 and P45 (Figure S4A). In WT ABX mice, only a trend toward decreased body weight was noted compared to WT CTRL (Figure S4A). In addition, we investigated the efficacy of ABX treatment and found a significant decrease of bacterial DNA concentration in the feces of CDKL5 KO and WT mice after ABX administration compared to the respective controls (Figure S4B).

Both patients affected by CDD and CDKL5 null mice present a visual deficit.[2,33–36] After 13 days of ABX administration, we assessed the visual cortical responses by optical imaging of the intrinsic signal (IOS) (Figure 4B). As expected, CDKL5 KO CTRL showed a significant reduction in the amplitude of visual responses compared to WT CTRL (Figure 4C). Remarkably, ABX administration rescued the visual response impairment, bringing the signal amplitude back to the WT CTRL value (Figure 4C). As already observed by our group[37] ABX did not alter amplitude of visual neuronal responses when administered to WT animals (Figure 4C).

Subsequently, we explored whether ABX-driven manipulation of the gut microbiota could improve behavioral impairments in CDD mice. First, we investigated nest building (Figure 4D), an instinctive/spontaneous behavior. Mice are highly motivated to build a nest as it has functions related to survival and reproduction, including regulating body temperature, protecting from predators or aggressive cage mates, sheltering from cold, and increasing litter survival.[38] CDKL5 KO CTRL mice showed impaired nest-building behavior compared to WT CTRL and WT ABX animals (Figure 4E). However, ABX treatment failed to improve nest-building scores in the mutants and did not affect the performance of the WT mice (Figures 4E and S5). Then, we scored hindlimb clasping (Figure 4F), which is a signature of altered motor coordination and has been previously observed in CDKL5 KO mice.[39] As expected, CDKL5 KO CTRL mice exhibited a certain deficit in motor coordination compared to the WT CTRL group (Figure 4G). However, ABX treatment neither improved the phenotype in KO mice nor influenced the behavior of WT mice (Figure 4G).

Finally, we assessed exploration using the Y-maze (Figure 3H). CDKL5 KO CTRL mice performed a higher number of total entries than WT CTRL mice (Figure 4I) and displayed an increase in total distance moved and velocity (Figures 4J and 4K). This hyperactive phenotype was normalized to the level of WT mice by manipulating the gut microbiota using ABX (Figures 4I–4K). Importantly, the ABX administration did not disrupt the WT performance (Figures 4I–4L). In addition, CDKL5 KO CTRL mice performed worse than their WT littermates in the percentage of alternation in the three arms but the ABX did not normalize this impairment (Figure 4L).

In summary, targeting gut microbiota alterations in CDKL5 deficient mice was able to improve functional properties of cortical neurons, and ameliorated specific behavioral abnormalities.

ABX-driven gut microbiota manipulation influence microglia phenotype in CDKL5 KO mice

The intestinal microbiota has emerged as a significant factor influencing the maturation, differentiation, and functionality of microglia cells.[40,41] Interestingly, microglia from CDKL5 mutants displayed a phenotype typical of an activation state.[42] Thus, based on this information, we explored whether ABX, which manipulates gut microbiota composition, could ameliorate the potential state of neuroinflammation in the CDKL5 KO brain by acting on microglia cells.

Three-dimensional morphological analysis of microglia cell bodies in the visual cortex (Figure 5A) indicated no significant changes in soma area or volume in CDKL5 KO CTRL and WT CTRL mice (Figures 5B and 5C). However, ABX treatment significantly decreased both soma area and volume in WT and CDKL5 KO mice compared to the respective CTRL groups (Figures 5B and 5C). In addition, CDKL5 KO CTRL mice displayed a

(N) Representative histopathological examination of H&E stained colon tissue section of WT and KO mice (magnification 4×; scale bar, 100 μm).
(O–R) Histopathological analysis of WT versus KO colon sections (n = 7–9 mice/group). (O) Muscle width (μm) (unpaired t test $^{**}p = 0.004$). (P) Crypt layer depth (μm) (unpaired t test $^{*}p = 0.033$). (Q) Villi length (μm) and (R) width (μm) (villi length unpaired t tests $p = 0.272$; villi width unpaired t test $p = 0.893$).
Error bars represent SEM. Circles represent single experimental subjects.

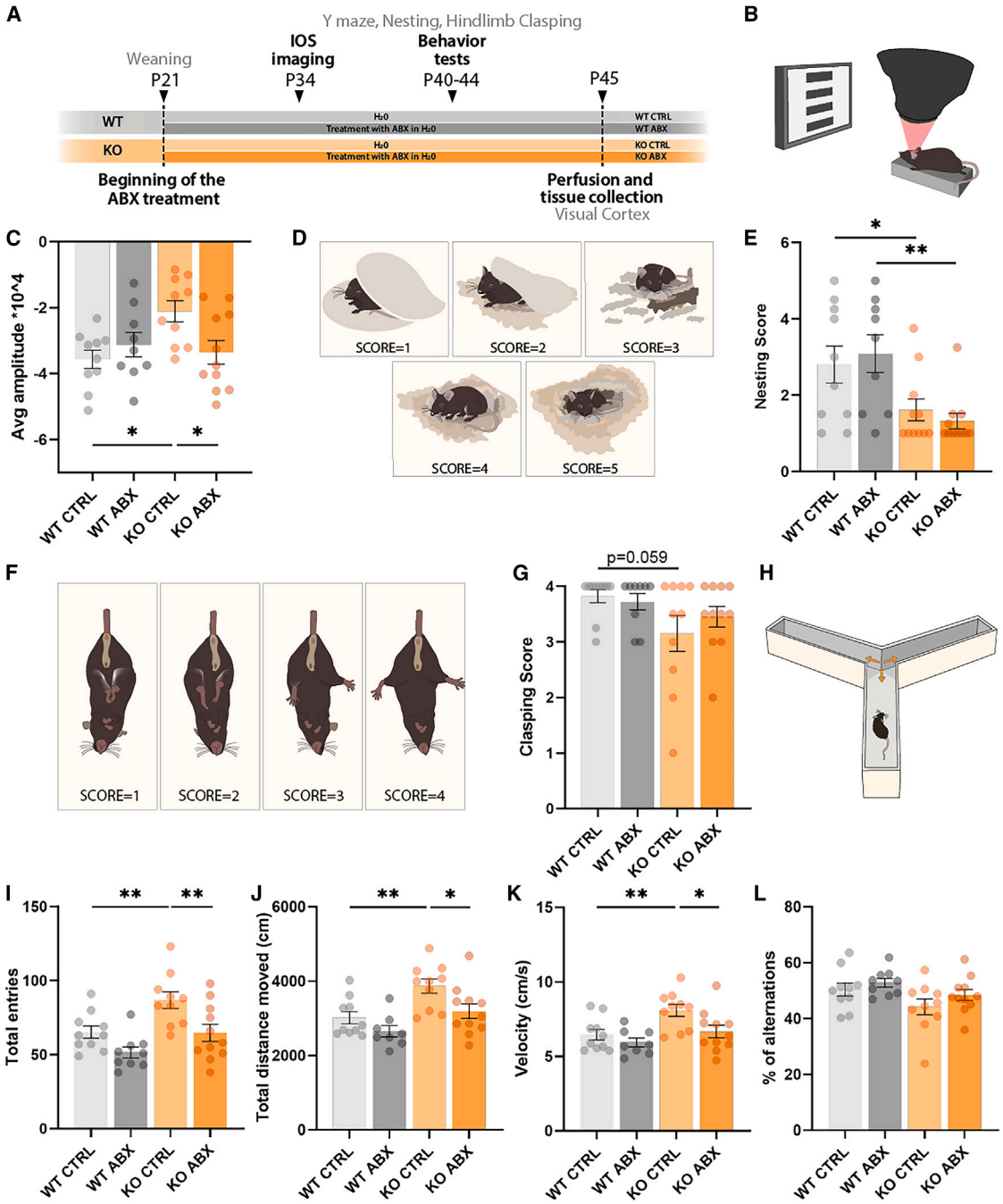

Figure 4. ABX administration significantly improves visual cortical responses and reduces the hyperactive behavior of CDKL5 KO mice

(A) Experimental timeline. Mice were single housed starting from weaning (P21) onward. A battery of behavioral and functional tests was performed (n = 9–11 animals/group). Groups: WT control group (WT CTRL), WT ABX-treated group (WT ABX), CDKL5 KO control group (KO CTRL), and CDKL5 KO ABX-treated group (KO ABX).

(B) Schematic of the IOS imaging setup.

(C) The graph represents the average amplitude of the cortical responses to contralateral eye stimulation (two-way ANOVA genotype × treatment interaction p = 0.0162, multiple comparisons Sidak's *post hoc* test; WT CTRL versus KO CTRL *p = 0.019, KO CTRL versus KO ABX *p = 0.049).

(D) Schematic of the nest-building scoring system.

(E) Nest-building ability scored at 24 h after placement of the nestlet (two-way ANOVA genotype × treatment interaction p = 0.443, main effect of genotype p = 0.0003, multiple comparisons Sidak *post hoc* test; WT CTRL versus KO CTRL *p = 0.056, WT ABX versus KO ABX **p = 0.004).

(F) Schematic of the hindlimb clasping scoring system.

(legend continued on next page)

significant reduction in microglia sphericity in comparison with WT CTRL animals (Figure 5D). Notably, ABX administration rescued this feature only in CDKL5 KO mice, while it had no impact on sphericity in WT mice (Figure 5D). Since ameboid microglia lose the spherical shape of their cell body, a reduction in this characteristic might indicate that CDKL5 KO microglia are on the verge of activation in response to inflammatory signals, potentially emanating from an imbalanced microbiota. Administration of ABX may restore CDKL5 KO cells to a surveillance state.

To gain further insight on microglia function, we quantified their lysosomal content by CD68 staining (Figure 5E). Our analysis revealed that CDKL5 KO CTRL microglia exhibited elevated expression of CD68 compared to WT CTRL mice (Figure 5F). However, ABX administration did not affect CD68 levels in either the CDKL5 KO or WT group (Figure 5F). This piece of data may suggest a higher phagocytic capacity of CDKL5 KO microglia with respect to WT animals.

Then, microglia complexity (Figure 6A) was investigated by quantifying filament length, number of branching points, and number of terminal points. Intriguingly, CDKL5 KO CTRL microglia displayed a significant decrease in all of the above-mentioned parameters with respect to the WT CTRL group, and ABX administration completely rescued the phenotype (Figures 6B–6D). Sholl analysis further demonstrated a reduction in CDKL5 KO CTRL cell complexity, due to a decrease of intersection numbers at specific soma distances (Table S3), which was restored to WT levels by ABX treatment (Figures 6E–6G). Finally, ABX administration had no effect on microglia ramifications and complexity in WT mice (Figures 6B–6G).

Astrocytes are involved in neuroinflammation, and recent studies suggest they could play a role in the gut-microbiota-brain axis[43–46]; therefore, we quantified their density in the visual cortex. No differences were observed between WT and CDKL5 KO mice, and ABX treatment had no effect (Figure S6).

Overall, our investigation of microglia phenotype suggests a potential state of activation in the CDKL5 KO cerebral cortex that could be counteracted by manipulating the intestinal microbiota with the ABX.

Fecal microbiota transplantation transfers the CDKL5 KO phenotype to WT recipient mice

To provide further independent evidence to support the contribution of the CDKL5 KO microbiota to the phenotype of this mouse model, we performed a fecal transplantation (FT) experiment. Feces from CDKL5 KO or WT donors were transplanted in WT recipient animals (Figure 7A). Body weight was monitored throughout the FT experiments, showing no significant difference between the recipient groups (Figure S7). 12 days post FT, visual responses were assessed. Strikingly, KO-FT mice exhibited a reduced amplitude of visual responses compared to the control group that received feces from other WT mice (WT-FT, Figure 7B), mirroring the decrease in IOS imaging responses observed in CDKL5 KO animals (Figure 4C). Additionally, KO-FT mice displayed a significant increase in total entries into the Y-maze arms compared to WT-FT (Figure 7C), mirroring the behavior of the CDKL5 KO group (Figure 4I). However, no differences were observed in total distance moved, velocity, or percentage of alternation (Figures 7D–7F).

The FT results further underscore the key role of the gut microbiota in shaping behavior and cortical responses in the CDD mouse model, and they demonstrate that FT is an effective tool for transferring neurological phenotypes.

DISCUSSION

Our investigation identified distinct variations in the developmental maturation pattern of the intestinal microbiota between two CDD mouse models and their WT littermates. As expected from the influence of various factors, including genetics, diet, and lifestyle, on the gut microbiota composition,[47] the alterations present in CDD mice were affected by the specific model, age, and facility. However, we found a noteworthy CDD microbial signature characterized by dysregulated bacterial taxa that were consistently altered regardless of facility.

In both the Pisa and Berlin facilities, the major distinctions between CDKL5 KO animals and WT littermates were observed at juvenile ages. Alpha diversity was decreased at P25 and P32 in the Berlin vivarium, and a tendency for a decrease was observed in Pisa at the same ages. Similarly, in an Italian cohort of patients affected by CDD, fecal microbiota alpha diversity was diminished compared to healthy individuals.[16] The Pisa CDKL5 KO mouse also displayed specific alterations in the gut microbiota: taxa belonging to the phylum Proteobacteria were significantly enriched in these mice, at both P25 and P32 (i.e., orders Burkholderiales, Pasteurellales, families Enterobacteriaceae, Alcaligenaceae, genus *Sutterella*). These microbes were suggested as potential markers of microbiota instability and thus as a predisposition to disease onset.[28] Blooming of Proteobacteria has been associated with various disease conditions, such as IBD, metabolic disorders and non-alcoholic fatty liver disease (NAFLD).[27] Indeed, the Enterobacteriaceae family is increased

(G) Scoring obtained upon 2 min of tail suspension (two-way ANOVA genotype × treatment interaction $p = 0.342$, main effect of genotype $p = 0.032$, multiple comparisons Sidak *post hoc* test; WT CTRL versus KO CTRL $p = 0.059$).
(H) Schematic of the Y-maze arena.
(I) Y-maze number of total entries (two-way ANOVA genotype × treatment interaction $p = 0.419$, main effect of genotype $p = 0.001$, main effect of treatment $p = 0.001$, multiple comparisons Sidak's *post hoc* test; WT CTRL versus KO CTRL $^{**}p = 0.009$, KO CTRL versus KO ABX $^{**}p = 0.006$).
(J) Y-maze total distance moved in centimeters (two-way ANOVA genotype × treatment interaction $p = 0.403$, main effect of genotype $p = 0.0006$, main effect of treatment $p = 0.008$, multiple comparisons Sidak's *post hoc* test; WT CTRL versus KO CTRL $^{**}p = 0.004$, KO CTRL versus KO ABX $^{*}p = 0.021$).
(K) Velocity (cm/s) in the Y-maze (two-way ANOVA genotype × treatment interaction $p = 0.250$, main effect of genotype $p = 0.004$, main effect of treatment $p = 0.016$, multiple comparisons Sidak's *post hoc* test; WT CTRL versus KO CTRL $^{**}p = 0.008$, KO CTRL versus KO ABX $^{*}p = 0.020$).
(L) % of alterations in the arms (two-way ANOVA genotype × treatment interaction $p = 0.688$, main effect of genotype $p = 0.024$, multiple comparisons Sidak's *post hoc* test, no significant difference).
Error bars represent SEM. Circles represent single experimental subjects.

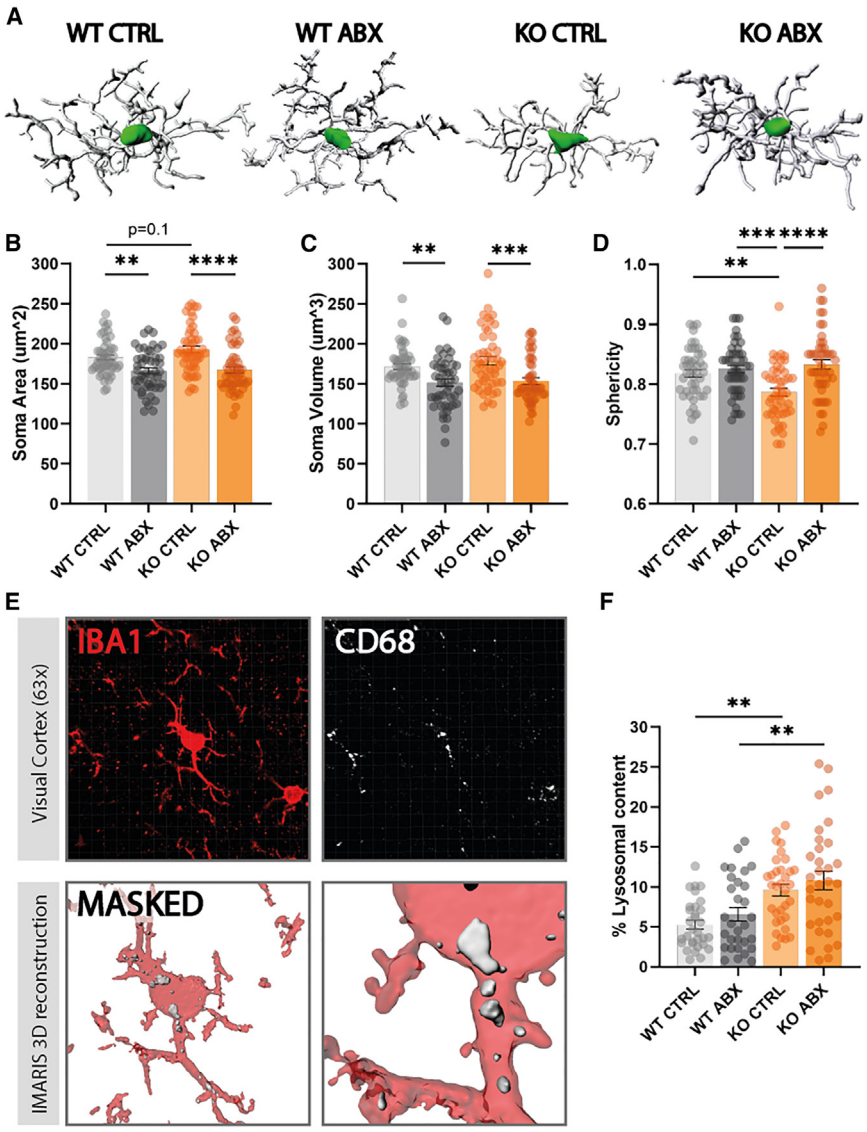

Figure 5. Microglia soma shape analysis and expression of the lysosomal marker CD68 in CDKL5 KO mice visual cortex and effects of ABX administration

(A) Three-dimensional soma shape reconstruction of representative microglial cells from each experimental group.

(B) Microglia soma area (um^2) (two-way ANOVA genotype × treatment interaction $p = 0.236$, main effect of treatment $p < 0.0001$, multiple comparisons Sidak's *post hoc* test; WT CTRL versus KO CTRL $p = 0.117$, WT CTRL versus WT ABX $^{**}p = 0.004$, KO CTRL versus KO ABX $^{****}p < 0.0001$).

(C) Microglia soma volume (um^3) (two-way ANOVA genotype × treatment interaction $p = 0.537$, main effect of treatment $p < 0.0001$, multiple comparisons Sidak's *post hoc* test; WT CTRL versus WT ABX $^{**}p = 0.003$, KO CTRL versus KO ABX $^{***}p = 0.0001$).

(D) Microglia sphericity (two-way ANOVA genotype × treatment interaction $p = 0.004$, main effect of treatment $p = 0.0001$, main effect of genotype $p = 0.085$, multiple comparisons Sidak's *post hoc* test; WT CTRL versus KO CTRL $^{**}p = 0.008$, KO CTRL versus WT ABX $^{***}p = 0.005$, KO CTRL versus KO ABX $^{****}p < 0.0001$).

(E) Representative volumes reconstruction of IBA1- and CD68-immunostained microglia.

(F) % of lysosomal content in IBA-1 immunostained microglia (two-way ANOVA genotype × treatment interaction $p = 0.875$, main effect of genotype $p < 0.0001$, multiple comparisons Sidak's *post hoc* test; WT CTRL versus KO CTRL $^{**}p = 0.001$, WT ABX versus KO ABX $^{**}p = 0.0006$). Error bars represent SEM. Circles represent single cells. Microglia soma shape analysis: $n = 8$ cells/animal/experimental group corresponding to $n = 6$ animals/experimental group. CD68 levels: $n = 5$ cells/animal/experimental group corresponding to $n = 6$ animals/experimental group.

in patients with type 2 diabetes,[48] and the class Gammaproteobacteria was increased in children affected by NAFLD with respect to healthy controls.[49] In addition, an enrichment of Proteobacteria has been found in mouse models of IBD,[50–52] suggesting a potential state of intestinal inflammation in the CDD mouse model. Notably, we observed an increase in clusters of infiltrating monocytes in the colon of CDKL5 KO mice from the Pisa vivarium. This immune cell infiltration was accompanied by structural changes, including a reduction in crypt depth and an increase in muscle layer width, as well as elevated *tff3* gene expression. TFF3 plays a role in the first line physiological response to an inflammatory environment, increasing the expression of *tjp1* and *cldn1* to restore gut homeostasis and/or barrier function.[53–55] This altered intestinal state could be linked to pro-inflammatory bacteria taxa in the microbiota.

Recent reports have linked Proteobacteria to the modulation of the gut-brain axis. A significant increase in gut Proteobacteria associated with neuroinflammation, and accompanied by exploration impairment and anxiety-like behavior was observed in a mouse model of diet induced obesity.[56] Importantly, an enrichment in Enterobacteriaceae was observed in patients affected by CDD and manifesting severe GI disturbances compared to patients with mild to normal GI features,[16] indicating similarities in the gut microbiota profile of mouse model and human subjects.

While the CDKL5 KO mice from the Berlin vivarium displayed no differences at P32 compared to WT littermates, they showed enrichment in the Bacteroidaceae family at P25, which was also found in the Pisa CDKL5 KO mouse colony, demonstrating a common feature of the CDD microbiota. The expansion of Bacteroidaceae has been associated with colitis in mouse models,[57,58] inflammation in patients with chirrosis,[59] Alzheimer disease, and IBD patients.[60] Therefore, the blooming of Bacteroidaceae could be an early sign of gut microbiota imbalance in the CDD mouse. On the other hand, *B. longum* was underrepresented in the two CDD mouse models compared to their WT

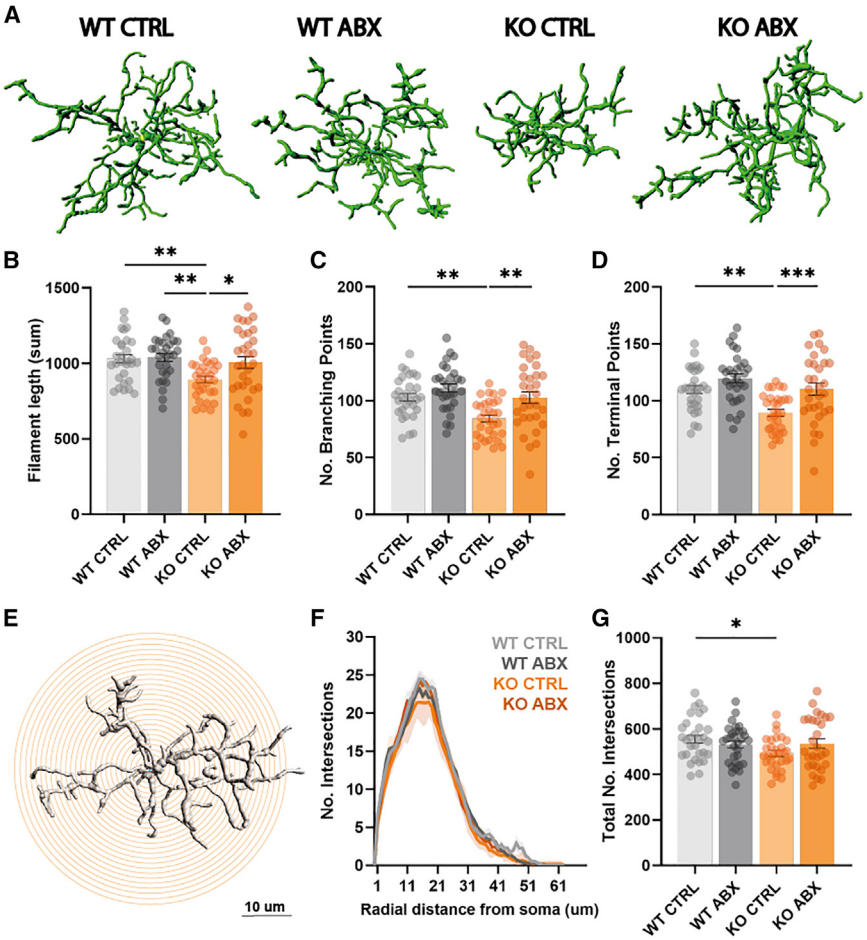

Figure 6. ABX treatment rescues microglia arborization and complexity in CDKL5 KO mice

(A) Three-dimensional reconstruction of representative microglia arborization from each experimental group.

(B) Filament length (sum) (two-way ANOVA genotype × treatment interaction $p = 0.075$, main effect of genotype $p = 0.004$, main effect of treatment $p = 0.038$, multiple comparisons Sidak's *post hoc* test; WT CTRL versus KO CTRL $^{**}p = 0.007$, KO CTRL versus WT ABX $^{**}p = 0.003$, KO CTRL versus KO ABX $^{*}p = 0.038$).

(C) Number of branching points (two-way ANOVA genotype × treatment interaction $p = 0.178$, main effect of genotype $p = 0.0006$, main effect of treatment $p = 0.0008$, multiple comparisons Sidak's *post hoc* test; WT CTRL versus KO CTRL $^{**}p = 0.001$, KO CTRL versus KO ABX $^{**}p = 0.001$).

(D) Number of terminal points (two-way ANOVA genotype × treatment interaction $p = 0.187$, main effect of genotype $p = 0.0003$, main effect of treatment $p = 0.0003$, multiple comparisons Sidak's *post hoc* test; WT CTRL versus KO CTRL $^{**}p = 0.001$, KO CTRL versus KO ABX $^{***}p = 0.009$).

(E) Representative image of a Sholl analysis in reconstructed IBA1-immunostained microglia.

(F) Sholl analysis of microglia. (two-way ANOVA distance × experimental_group interaction $p = 0.998$, distance factor $p < 0.0001$, experimental_group factor $p < 0.0001$).

(G) Total number of intersections (two-way ANOVA genotype × treatment interaction $p = 0.046$, main effect of genotype $p = 0.084$, multiple comparisons Sidak's *post hoc* test; WT CTRL versus KO CTRL $^{*}p = 0.053$).

Error bars represent SEM. Circles represent single cells. $n = 5$ cells/animal/experimental group corresponding to $n = 6$ animals/experimental group.

littermates at P70. Multiple strains of *B. longum* have been formulated as probiotics due to their ability to elicit various health benefits. They have demonstrated efficacy in conditions such as IBD, cardiovascular diseases, respiratory illnesses, anxiety, depression, and cognitive functions.[61] Therefore, the reduction of *B. longum* in our CDD mouse models suggests a potential imbalance in the composition of gut microbes, characterized by a deficiency of beneficial bacteria that are crucial for maintaining intestinal homeostasis.

To further dissect additional shared taxa between the Pisa and Berlin CDD mouse models, we performed LEfSe analysis subtracting the variable "mouse facility." This analysis highlighted the order Burkholderiales and Bacteroidales, which are commonly enriched in the P25 CDKL5 KO mouse. In particular, *B. rodentium* was increased in CDKL5 KO at both P25 and P32, but no specific effects of this taxa on the gut-microbiota-brain axis have been reported so far. Among the common taxa decreased at P70, we found *Allobaculum*. *Allobaculum* is considered a beneficial microorganism, especially in the context of hypertension, and it is negatively correlated with colonic expression of anti-inflammatory genes such as FOXP3 and IL-10.[62,63]

In summary, our multi-site experiment showed an interaction between mouse genetics (i.e., the absence of CDKL5 protein) and environmental conditions (i.e., two different and geographically distant facilities) in shaping the intestinal microbiota. Previous studies suggest that the environment dominates over genetics[64] in determining the gut microbiota composition, and our results largely confirm this finding. As the DNA was extracted from all the fecal samples simultaneously and the sequencing was performed at the same time, we could exclude differences due to the sample processing. On the other hand, the standard chow used in the two facilities, the type of bedding, and/or other environmental factors could explain the dissimilarities between the Pisa and Berlin mice. Our efforts to identify microorganisms that are consistently altered in the CDKL5 KO mouse model revealed distinct taxa at specific ages. These taxa could be regarded as the CDKL5 KO signature microbes, suggesting a possible influence of genetics and indicating that the absence of functional CDKL5 might specifically shape the composition of the gut microbiota. The mechanisms by which impaired CDKL5 functions could influence the maturation or growth of specific microorganisms is still unknown and may suggest a role for

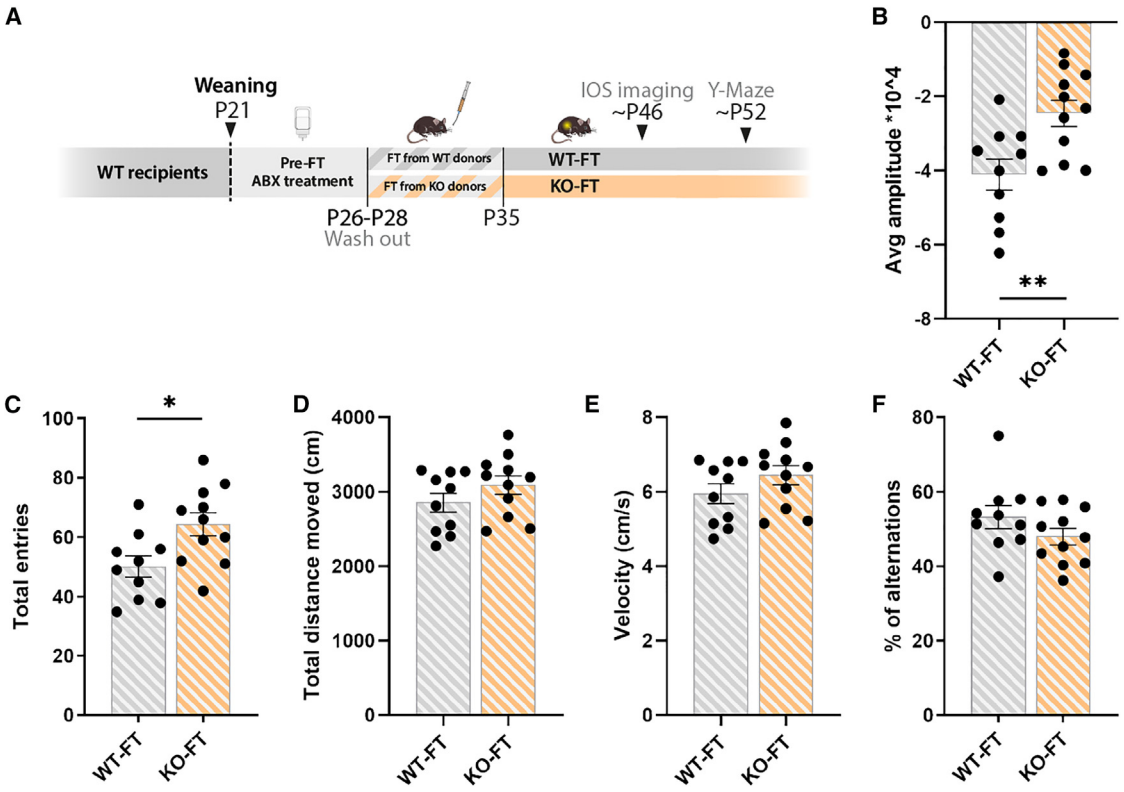

Figure 7. Fecal transplantation transfers the CDKL5 KO phenotype into WT recipient mice

(A) Experimental timeline of the FT experiment.

(B) Average amplitude of the cortical responses to contralateral eye stimulation (unpaired t test $^{**}p = 0.006$).

(C–F) Y-maze task results. (C) Number of total entries (unpaired t test $^{*}p = 0.015$). (D) Total distance moved in centimeters (unpaired t test $p = 0.201$). (E) Velocity (cm/s) (unpaired t test $p = 0.198$). (F) % of alterations in the arms (unpaired t test $p = 0.183$).

Error bars represent SEM. Circles represent single experimental subjects. $N = 10–11$ mice/experimental group.

CDKL5 in the enteric nervous system or in different types of intestinal cells.

Treating gut microbiota alterations in CDKL5 KO mice improved phenotypical impairment

The presence of a pro-inflammatory dysbiotic microbial community in CDD mice raises the intriguing possibility that the intestinal microbiota of CDD mice may contribute to the phenotype in these animals. Our results showing that several phenotypes are ameliorated by the administration of an antibiotic treatment to CDKL5 KO mice support this possibility. In particular, administration of ABX was able to improve visual response amplitude in CDKL5 KO mice. Visual alterations, also known as cortical visual impairment (CVI), were found to be present in 75% of patients with CDD. CVI correlates with reduced achievement of milestones and is a major feature of CDD that can impact on the quality of life and neurodevelopmental outcome of affected individuals.[3,35] In particular, visual acuity, a quantifiable measure of visual function, has been found to be altered in CDD mice.[33] The extent of impairment in visual acuity is linked to patients' gross motor ability, suggesting that it can be used as an outcome measure in both pre-clinical and clinical studies of CDD.[65] Improving this key symptom by targeting intestinal microbiota imbalance emphasizes the impact of abnormal gut-brain interaction in CDD beyond GI dysfunction.

ABX had no effects on nest-building behavior in CDKL5 KO mice. Nest building is an intricate innate behavior observed in both male and female mice. It requires the mouse to identify, gather, and process materials to create a functional shelter. CDKL5 KO mice show significant impairments in nest building, often leaving the materials untouched. Manipulating the microbiota with ABX did not improve the complex behavioral steps involved in nest building, nor did it increase the inclination toward this behavior. This suggests that nest building, which involves executive functions, is not ameliorated by ABX treatment.[66] While ABX administration did not affect working memory in the Y-maze, as indicated by unchanged percentage of alternation in both WT and CDKL5 KO-treated groups, it did normalize total entries, distance, and velocity in CDKL5 KO animals to WT levels. This suggests that intestinal microbiota alterations may be linked to the behavioral impulsivity observed in CDKL5 KO mice.[67] ABX administration appears to mitigate this hyperactive behavior. Although the mechanism is unclear, it may involve microglia cell abnormalities, as microglia have been implicated in hyperactive behavior in rodents[68] and the severity of attention-deficit hyperactivity disorder in humans.[69]

A major challenge in gut-brain axis studies is uncovering the cellular mechanisms and potential mediators by which gut microbiota influence distal tissues. Given that subclinical inflammation has been observed in patients with CDD, and a crosstalk between peripheral and central inflammatory processes has been proposed, we explored microglia cell behavior. Microglia, the predominant immune cells in the brain parenchyma, play a key role in neuroinflammation.[70] Nevertheless, they are involved in synaptic remodeling and plasticity of neuronal circuits.[71–76] Intriguingly, gut signals seem to influence microglia morphology and function,[37,40,41,77] and, in the CDKL5 KO mouse, microglia cells are in a state of activation.[42] We confirmed this result by observing a decrease in soma sphericity and an increase in lysosomal content in CDKL5 KO mice. Importantly, counteracting intestinal microbe imbalance increased the cell-body sphericity in CDKL5 KO to the level of WT mice. Finally, other microglia features linked to ramification complexity were found to be altered in CDKL5 KO animals. ABX treatment completely rescued this morphological phenotype, which could be linked to the ability of microglia to sense and surveil the surrounding environment and thus prevent potential harmful pathogens/molecules or maladaptive activation of the neuronal network. ABX had only limited effects on microglia shape in WT mice, in line with a previous report where authors did not observe significant changes in microglia density or morphology.[78]

Although ABX treatment rescued several phenotypes in the CDD mouse model, this approach alone does not directly confirm that the compensatory effects result from gut microbiota manipulation or the subsequent microbial signals to the brain. To establish a more direct link between gut microbes and the observed phenotypes, we employed a complementary approach: fecal microbiota transplantation. This method allows for the transfer of a specific phenotype via the intestinal microbiota, providing stronger evidence for a causal relationship between microbial composition and physiological or behavioral traits. In this study, FT from CDKL5 KO donors to WT recipients successfully induced key neurological deficits characteristic of the CDKL5 KO phenotype. These findings highlight the critical role of gut microbial signals in modulating both behavioral and brain functional outcomes, further emphasizing the microbiota influence on neurodevelopmental disorders.

Translational perspectives in targeting the intestinal microbiota in CDD

Our study underscores the potential efficacy of targeting the gut microbiota to alleviate the symptoms of CDD. Employing a multi-site approach, we identified intestinal microbiota alterations in CDD mouse models that mirrors the differences observed in patients. The presence of potentially pro-inflammatory taxa (e.g., Bacteroidaceae, Enterobacteriaceae) and a decrease in beneficial bacteria, such as *B. longum*, could contribute to an inflammatory state that activates microglial cells and impacts the severity of neurological symptoms. The ABX treatment improved neurological outcomes and microglia morphology, indicating partial relief from potential CDD-related inflammation. Notably, intestinal inflammation in humans has been linked to seizures and altered responsiveness to anti-seizure medication.[79] This is a key aspect to consider in people with CDD who are affected by refractory epilepsy who have subclinical smoldering inflammation[6] and immune dysregulation.[5] Our findings, therefore, suggest harnessing the modifiable factor of gut microbiota as a novel target to alleviate symptom severity by mitigating peripheral and potentially brain low-grade inflammation. Easily applicable approaches such as probiotics tailored to the CDD fecal microbiota profile, prebiotics, and dietary supplements could offer almost side-effect-free interventions. Moreover, promising results have been obtained in ameliorating both neurological and GI symptoms in people with ASD via FT,[80–82] which, based on our investigation, could be conceivable for patients affected by CDD.

In conclusion, our pioneering exploration of the gut-microbiota-brain axis in CDD unveils promising avenues for novel therapeutic strategies. We propose transformative treatments based on targeting the intestinal microbiota that hold the potential to alleviate symptoms and improve the overall well-being of patients with CDD.

Limitations of the study

We acknowledge that this study did not assess other relevant behavioral phenotypes, such as emotional and social behaviors, which have previously been linked to gut microbiota modulation[83,84] and have been shown to be altered in the CDKL5 KO mouse model.[85–88]

Additionally, single housing may influence gut microbiota composition and physiological parameters, as previously documented.[89,90] Future studies should consider alternative housing strategies, such as co-housing post weaning, to mitigate these effects while maintaining experimental rigor.

RESOURCE AVAILABILITY

Lead contact

Requests for further information, resources, and reagents should be directed to and will be fulfilled by the lead contact, Paola Tognini (paola.tognini@santannapisa.it).

Material availability

This study did not generate unique reagents.

Data and code availability

- 16S rRNA-seq data generated in this study have been deposited in the NCBI Sequence Read Archive (SRA) and are available at Zenodo.[91] The accession number is listed in the key resource table.
- The algorithms used for data analysis have been published at Zenodo and are described in the STAR Methods. The DOI is available in the key resource table.
- Any additional information required to reanalyze the data reported in this paper is available from the lead contact upon request.

ACKNOWLEDGMENTS

We thank the members of Tognini's team for insightful comments and feedback. Special thanks to Valentino Totaro and Raffaele Mazziotti for their support with Python, and to Beatrice Lecci and Francesco Calia for help in the revision. We thank Gioacchino Incandela, Francesca Biondi, and Dr. Silvia Burchielli for their help in the mouse facility. The graphical abstract was

created using https://BioRender.com. This research was supported by Telethon Grant GSP21001, Jerome Lejeune Advanced Grant 2022, NextGenerationEU Italian Ministry of University and Research M4.C2 -PNRR YOUNG MSCA_0000081 iNsPIReD, and PRIN-PNRR2022 CARE P2022CXN7X CUP I53D23006920001 to P.T. T.P. was supported by Intesa Sanpaolo Charity Fund, NextGenerationEU PNRR THE CUP I53C22000780001, and PRIN2022 20228RMXBE.

AUTHOR CONTRIBUTIONS

F.D. performed all the experiments, analyzed the data, and prepared the figures. M.G.G. performed H&E, immunofluorescence staining, qPCR, and microglia reconstruction. S.C. collected and extracted DNA from feces and analyzed the 16S rRNA-seq data. E.P. maintained the mouse colony and performed genotyping. A.T. helped in behavioral experiments. V.S. and V.M.K. collected the feces at the Berlin facility. T.P. participated in the experimental design and data interpretation. T.P. and V.M.K. gave feedback on the manuscript. P.T. conceived the project, supervised the experiments, interpreted the data, and wrote the manuscript.

DECLARATION OF INTERESTS

The authors declare no competing interests.

STAR★METHODS

Detailed methods are provided in the online version of this paper and include the following:

- KEY RESOURCES TABLE
- EXPERIMENTAL MODEL AND STUDY PARTICIPANT DETAILS
  - Animals
- METHOD DETAILS
  - Fecal DNA extraction and 16S rRNA sequencing
  - Fecal water content
  - Defecation frequency test and whole gut transit time measurement
  - RNA extraction and qPCR
  - Hematoxylin and eosin (H&E) staining
  - Antibiotic treatment
  - Optical imaging of the intrinsic signal (IOS)
  - Fecal transplantation
  - Behavioral analysis
  - Immunofluorescence analysis
- QUANTIFICATION AND STATISTICAL ANALYSIS

SUPPLEMENTAL INFORMATION

Supplemental information can be found online at https://doi.org/10.1016/j.celrep.2025.115546.

Received: July 16, 2024
Revised: January 31, 2025
Accepted: March 19, 2025
Published: April 10, 2025

REFERENCES

1. Jakimiec, M., Paprocka, J., and Śmigiel, R. (2020). CDKL5 Deficiency Disorder—A Complex Epileptic Encephalopathy. Brain Sci. *10*, 107. https://doi.org/10.3390/brainsci10020107.
2. Leonard, H., Downs, J., Benke, T.A., Swanson, L., Olson, H., and Demarest, S. (2022). CDKL5 deficiency disorder: clinical features, diagnosis, and management. Lancet Neurol. *21*, 563–576.
3. Demarest, S.T., Olson, H.E., Moss, A., Pestana-Knight, E., Zhang, X., Parikh, S., Swanson, L.C., Riley, K.D., Bazin, G.A., Angione, K., et al. (2019). CDKL5 deficiency disorder: Relationship between genotype, epilepsy, cortical visual impairment, and development. Epilepsia *60*, 1733–1742.
4. Mangatt, M., Wong, K., Anderson, B., Epstein, A., Hodgetts, S., Leonard, H., and Downs, J. (2016). Prevalence and onset of comorbidities in the CDKL5 disorder differ from Rett syndrome. Orphanet J. Rare Dis. *11*, 39.
5. Leoncini, S., De Felice, C., Signorini, C., Zollo, G., Cortelazzo, A., Durand, T., Galano, J.-M., Guerranti, R., Rossi, M., Ciccoli, L., and Hayek, J. (2015). Cytokine Dysregulation in MECP2- and CDKL5-Related Rett Syndrome: Relationships with Aberrant Redox Homeostasis, Inflammation, and ω-3 PUFAs. Oxid. Med. Cell. Longev. *2015*, 421624.
6. Cortelazzo, A., de Felice, C., Leoncini, S., Signorini, C., Guerranti, R., Leoncini, R., Armini, A., Bini, L., Ciccoli, L., and Hayek, J. (2017). Inflammatory protein response in CDKL5-Rett syndrome: evidence of a subclinical smouldering inflammation. Inflamm. Res. *66*, 269–280.
7. Saurman, V., Margolis, K.G., and Luna, R.A. (2020). Autism Spectrum Disorder as a Brain-Gut-Microbiome Axis Disorder. Dig. Dis. Sci. *65*, 818–828.
8. McElhanon, B.O., McCracken, C., Karpen, S., and Sharp, W.G. (2014). Gastrointestinal symptoms in autism spectrum disorder: a meta-analysis. Pediatrics *133*, 872–883.
9. Doshi-Velez, F., Ge, Y., and Kohane, I. (2014). Comorbidity clusters in autism spectrum disorders: an electronic health record time-series analysis. Pediatrics *133*, e54–e63.
10. Richdale, A.L., and Schreck, K.A. (2009). Sleep problems in autism spectrum disorders: prevalence, nature, & possible biopsychosocial aetiologies. Sleep Med. Rev *13*, 403–411.
11. Damiani, F., Cornuti, S., and Tognini, P. (2023). The gut-brain connection: Exploring the influence of the gut microbiota on neuroplasticity and neurodevelopmental disorders. Neuropharmacology *231*, 109491.
12. Murakami, M., and Tognini, P. (2019). The Circadian Clock as an Essential Molecular Link Between Host Physiology and Microorganisms. Front. Cell. Infect. Microbiol. *9*, 469.
13. Ding, X., Xu, Y., Zhang, X., Zhang, L., Duan, G., Song, C., Li, Z., Yang, Y., Wang, Y., Wang, X., and Zhu, C. (2020). Gut microbiota changes in patients with autism spectrum disorders. J. Psychiatr. Res. *129*, 149–159.
14. Borghi, E., Borgo, F., Severgnini, M., Savini, M.N., Casiraghi, M.C., and Vignoli, A. (2017). Rett Syndrome: A Focus on Gut Microbiota. Int. J. Mol. Sci. *18*, 344. https://doi.org/10.3390/ijms18020344.
15. Strati, F., Cavalieri, D., Albanese, D., De Felice, C., Donati, C., Hayek, J., Jousson, O., Leoncini, S., Pindo, M., Renzi, D., et al. (2016). Altered gut microbiota in Rett syndrome. Microbiome *4*, 41.
16. Borghi, E., Xynomilakis, O., Ottaviano, E., Ceccarani, C., Viganò, I., Tognini, P., and Vignoli, A. (2024). Gut microbiota profile in CDKL5 deficiency disorder patients. Sci. Rep. *14*, 7376.
17. Mitrea, L., Nemeş, S.-A., Szabo, K., Teleky, B.-E., and Vodnar, D.-C. (2022). Guts Imbalance Imbalances the Brain: A Review of Gut Microbiota Association With Neurological and Psychiatric Disorders. Front. Med. *9*, 813204.
18. Sultan, S., El-Mowafy, M., Elgaml, A., Ahmed, T.A.E., Hassan, H., and Mottawea, W. (2021). Metabolic Influences of Gut Microbiota Dysbiosis on Inflammatory Bowel Disease. Front. Physiol. *12*, 715506.
19. Yu, L.C.-H. (2018). Microbiota dysbiosis and barrier dysfunction in inflammatory bowel disease and colorectal cancers: exploring a common ground hypothesis. J. Biomed. Sci. *25*, 79.
20. Hamjane, N., Mechita, M.B., Nourouti, N.G., and Barakat, A. (2024). Gut microbiota dysbiosis -associated obesity and its involvement in cardiovascular diseases and type 2 diabetes. A systematic review. Microvasc. Res. *151*, 104601.
21. Thukral, A.K. (2017). A review on measurement of Alpha diversity in biology. Intern. J. Contemp. Microbiol. *54*, 1. https://doi.org/10.5958/2395-146x.2017.00001.
22. Pinart, M., Dötsch, A., Schlicht, K., Laudes, M., Bouwman, J., Forslund, S.K., Pischon, T., and Nimptsch, K. (2021). Gut Microbiome Composition

in Obese and Non-Obese Persons: A Systematic Review and Meta-Analysis. Nutrients *14*, 12. https://doi.org/10.3390/nu14010012.

23. Hirano, A., Umeno, J., Okamoto, Y., Shibata, H., Ogura, Y., Moriyama, T., Torisu, T., Fujioka, S., Fuyuno, Y., Kawarabayasi, Y., et al. (2018). Comparison of the microbial community structure between inflamed and non-inflamed sites in patients with ulcerative colitis. J. Gastroenterol. Hepatol. *33*, 1590–1597. https://doi.org/10.1111/jgh.14129.
24. Li, Z., Zhou, J., Liang, H., Ye, L., Lan, L., Lu, F., Wang, Q., Lei, T., Yang, X., Cui, P., and Huang, J. (2022). Differences in Alpha Diversity of Gut Microbiota in Neurological Diseases. Front. Neurosci. *16*, 879318.
25. Bray, J.R., and Curtis, J.T. (1957). An Ordination of the Upland Forest Communities of Southern Wisconsin.
26. Segata, N., Izard, J., Waldron, L., Gevers, D., Miropolsky, L., Garrett, W.S., and Huttenhower, C. (2011). Metagenomic biomarker discovery and explanation. Genome Biol. *12*, R60.
27. Rizzatti, G., Lopetuso, L.R., Gibiino, G., Binda, C., and Gasbarrini, A. (2017). Proteobacteria: A Common Factor in Human Diseases. BioMed Res. Int. *2017*, 9351507. https://doi.org/10.1155/2017/9351507.
28. Shin, N.-R., Whon, T.W., and Bae, J.-W. (2015). Proteobacteria: microbial signature of dysbiosis in gut microbiota. Trends Biotechnol. *33*, 496–503.
29. Yang, Y., Lin, Z., Lin, Q., Bei, W., and Guo, J. (2022). Pathological and therapeutic roles of bioactive peptide trefoil factor 3 in diverse diseases: recent progress and perspective. Cell Death Dis. *13*, 62.
30. Hoffmann, W. (2021). Trefoil Factor Family (TFF) Peptides and Their Links to Inflammation: A Re-evaluation and New Medical Perspectives. Int. J. Mol. Sci. *22*, 4909. https://doi.org/10.3390/ijms22094909.
31. Anand, N., Gorantla, V.R., and Chidambaram, S.B. (2022). The Role of Gut Dysbiosis in the Pathophysiology of Neuropsychiatric Disorders. Cells *12*, 54. https://doi.org/10.3390/cells12010054.
32. Morais, L.H., Schreiber, H.L., and Mazmanian, S.K. (2021). The gut microbiota–brain axis in behaviour and brain disorders. Nat. Rev. Microbiol. *19*, 241–255.
33. Mazziotti, R., Lupori, L., Sagona, G., Gennaro, M., Della Sala, G., Putignano, E., and Pizzorusso, T. (2017). Searching for biomarkers of CDKL5 disorder: early-onset visual impairment in CDKL5 mutant mice. Hum. Mol. Genet. *26*, 2290–2298.
34. Lupori, L., Sagona, G., Fuchs, C., Mazziotti, R., Stefanov, A., Putignano, E., Napoli, D., Strettoi, E., Ciani, E., and Pizzorusso, T. (2019). Site-specific abnormalities in the visual system of a mouse model of CDKL5 deficiency disorder. Hum. Mol. Genet. *28*, 2851–2861. https://doi.org/10.1093/hmg/ddz102.
35. Brock, D., Fidell, A., Thomas, J., Juarez-Colunga, E., Benke, T.A., and Demarest, S. (2021). Cerebral Visual Impairment in CDKL5 Deficiency Disorder Correlates With Developmental Achievement. J. Child Neurol. *36*, 974–980.
36. Quintiliani, M., Ricci, D., Petrianni, M., Leone, S., Orazi, L., Amore, F., Gambardella, M.L., Contaldo, I., Veredice, C., Perulli, M., et al. (2021). Cortical Visual Impairment in CDKL5 Deficiency Disorder. Front. Neurol. *12*, 805745.
37. Lupori, L., Cornuti, S., Mazziotti, R., Borghi, E., Ottaviano, E., Cas, M.D., Sagona, G., Pizzorusso, T., and Tognini, P. (2022). The gut microbiota of environmentally enriched mice regulates visual cortical plasticity. Cell Rep. *38*, 110212.
38. Deacon, R.M.J. (2006). Assessing nest building in mice. Nat. Protoc. *1*, 1117–1119.
39. Amendola, E., Zhan, Y., Mattucci, C., Castroflorio, E., Calcagno, E., Fuchs, C., Lonetti, G., Silingardi, D., Vyssotski, A.L., Farley, D., et al. (2014). Mapping pathological phenotypes in a mouse model of CDKL5 disorder. PLoS One *9*, e91613.
40. Erny, D., Hrabě de Angelis, A.L., Jaitin, D., Wieghofer, P., Staszewski, O., David, E., Keren-Shaul, H., Mahlakoiv, T., Jakobshagen, K., Buch, T., et al. (2015). Host microbiota constantly control maturation and function of microglia in the CNS. Nat. Neurosci. *18*, 965–977.
41. Erny, D., Dokalis, N., Mezö, C., Castoldi, A., Mossad, O., Staszewski, O., Frosch, M., Villa, M., Fuchs, V., Mayer, A., et al. (2021). Microbiota-derived acetate enables the metabolic fitness of the brain innate immune system during health and disease. Cell Metab. *33*, 2260–2276.e7.
42. Galvani, G., Mottolese, N., Gennaccaro, L., Loi, M., Medici, G., Tassinari, M., Fuchs, C., Ciani, E., and Trazzi, S. (2021). Inhibition of microglia overactivation restores neuronal survival in a mouse model of CDKL5 deficiency disorder. J. Neuroinflammation *18*, 155.
43. Zhao, Y.-F., Wei, D.-N., and Tang, Y. (2021). Gut Microbiota Regulate Astrocytic Functions in the Brain: Possible Therapeutic Consequences. Curr. Neuropharmacol. *19*, 1354–1366.
44. Spichak, S., Donoso, F., Moloney, G.M., Gunnigle, E., Brown, J.M., Codagnone, M., Dinan, T.G., and Cryan, J.F. (2021). Microbially-derived short-chain fatty acids impact astrocyte gene expression in a sex-specific manner. Brain Behav. Immun. Health *16*, 100318.
45. Seo, D.-O., O'Donnell, D., Jain, N., Ulrich, J.D., Herz, J., Li, Y., Lemieux, M., Cheng, J., Hu, H., Serrano, J.R., et al. (2023). ApoE isoform- and microbiota-dependent progression of neurodegeneration in a mouse model of tauopathy. Science *379*, eadd1236.
46. Chandra, S., Di Meco, A., Dodiya, H.B., Popovic, J., Cuddy, L.K., Weigle, I.Q., Zhang, X., Sadleir, K., Sisodia, S.S., and Vassar, R. (2023). The gut microbiome regulates astrocyte reaction to Aβ amyloidosis through microglial dependent and independent mechanisms. Mol. Neurodegener. *18*, 45.
47. Parizadeh, M., and Arrieta, M.-C. (2023). The global human gut microbiome: genes, lifestyles, and diet. Trends Mol. Med. *29*, 789–801.
48. American Diabetes Association (2014). Diagnosis and classification of diabetes mellitus. Diabetes Care *37*, S81–S90.
49. Michail, S., Lin, M., Frey, M.R., Fanter, R., Paliy, O., Hilbush, B., and Reo, N.V. (2015). Altered gut microbial energy and metabolism in children with non-alcoholic fatty liver disease. FEMS Microbiol. Ecol. *91*, 1–9.
50. Carvalho, F.A., Koren, O., Goodrich, J.K., Johansson, M.E.V., Nalbantoglu, I., Aitken, J.D., Su, Y., Chassaing, B., Walters, W.A., González, A., et al. (2012). Transient inability to manage proteobacteria promotes chronic gut inflammation in TLR5-deficient mice. Cell Host Microbe *12*, 139–152.
51. Selvanantham, T., Lin, Q., Guo, C.X., Surendra, A., Fieve, S., Escalante, N.K., Guttman, D.S., Streutker, C.J., Robertson, S.J., Philpott, D.J., and Mallevaey, T. (2016). NKT Cell-Deficient Mice Harbor an Altered Microbiota That Fuels Intestinal Inflammation during Chemically Induced Colitis. J. Immunol. *197*, 4464–4472.
52. Maharshak, N., Packey, C.D., Ellermann, M., Manick, S., Siddle, J.P., Huh, E.Y., Plevy, S., Sartor, R.B., and Carroll, I.M. (2013). Altered enteric microbiota ecology in interleukin 10-deficient mice during development and progression of intestinal inflammation. Gut Microbes *4*, 316–324.
53. Lin, N., Xu, L.-F., and Sun, M. (2013). The protective effect of trefoil factor 3 on the intestinal tight junction barrier is mediated by toll-like receptor 2 via a PI3K/Akt dependent mechanism. Biochem. Biophys. Res. Commun. *440*, 143–149.
54. Olivo-Martínez, Y., Bosch, M., Badia, J., and Baldomà, L. (2023). Modulation of the Intestinal Barrier Integrity and Repair by Microbiota Extracellular Vesicles through the Differential Regulation of Trefoil Factor 3 in LS174T Goblet Cells. Nutrients *15*, 2437. https://doi.org/10.3390/nu15112437.
55. Barrett, K.E. (2005). A new twist on trefoils. Focus on "TFF3 modulates NF-{kappa}B and a novel regulatory molecule of NF-{kappa}B in intestinal epithelial cells via a mechanism distinct from TNF-{alpha. Am. J. Physiol. Cell Physiol. *289*, C1069–C1071.
56. Jeong, M.-Y., Jang, H.-M., and Kim, D.-H. (2019). High-fat diet causes psychiatric disorders in mice by increasing Proteobacteria population. Neurosci. Lett. *698*, 51–57.

57. Harrison, C.A., Laubitz, D., Ohland, C.L., Midura-Kiela, M.T., Patil, K., Besselsen, D.G., Jamwal, D.R., Jobin, C., Ghishan, F.K., and Kiela, P.R. (2018). Microbial dysbiosis associated with impaired intestinal Na/H exchange accelerates and exacerbates colitis in ex-germ free mice. Mucosal Immunol. *11*, 1329–1341.

58. Ariake, K., Ohkusa, T., Sakurazawa, T., Kumagai, J., Eishi, Y., Hoshi, S., and Yajima, T. (2000). Roles of mucosal bacteria and succinic acid in colitis caused by dextran sulfate sodium in mice. J. Med. Dent. Sci. *47*, 233–241.

59. Piñero, F., Vazquez, M., Baré, P., Rohr, C., Mendizabal, M., Sciara, M., Alonso, C., Fay, F., and Silva, M. (2019). A different gut microbiome linked to inflammation found in cirrhotic patients with and without hepatocellular carcinoma. Ann. Hepatol. *18*, 480–487.

60. Wang, D., Zhang, X., and Du, H. (2022). Inflammatory bowel disease: A potential pathogenic factor of Alzheimer's disease. Prog. Neuropsychopharmacol. Biol. Psychiatry *119*, 110610.

61. Mills, S., Yang, B., Smith, G.J., Stanton, C., and Ross, R.P. (2023). Efficacy of alone or in multi-strain probiotic formulations during early life and beyond. Gut Microbes *15*, 2186098.

62. Dan, X., Mushi, Z., Baili, W., Han, L., Enqi, W., Huanhu, Z., and Shuchun, L. (2019). Differential Analysis of Hypertension-Associated Intestinal Microbiota. Int. J. Med. Sci. *16*, 872–881.

63. Richards, E.M., Pepine, C.J., Raizada, M.K., and Kim, S. (2017). The Gut, Its Microbiome, and Hypertension. Curr. Hypertens. Rep. *19*, 36.

64. Rothschild, D., Weissbrod, O., Barkan, E., Kurilshikov, A., Korem, T., Zeevi, D., Costea, P.I., Godneva, A., Kalka, I.N., Bar, N., et al. (2018). Environment dominates over host genetics in shaping human gut microbiota. Nature *555*, 210–215.

65. Olson, H.E., Costantini, J.G., Swanson, L.C., Kaufmann, W.E., Benke, T.A., Fulton, A.B., Hansen, R., Poduri, A., and Heidary, G. (2021). Cerebral visual impairment in CDKL5 deficiency disorder: vision as an outcome measure. Dev. Med. Child Neurol. *63*, 1308–1315.

66. Torres-Lista, V., and Giménez-Llort, L. (2013). Impairment of nesting behaviour in 3xTg-AD mice. Behav. Brain Res. *247*, 153–157.

67. Viglione, A., Sagona, G., Carrara, F., Amato, G., Totaro, V., Lupori, L., Putignano, E., Pizzorusso, T., and Mazziotti, R. (2022). Behavioral impulsivity is associated with pupillary alterations and hyperactivity in CDKL5 mutant mice. Hum. Mol. Genet. *31*, 4107–4120.

68. Rosin, J.M., Vora, S.R., and Kurrasch, D.M. (2018). Depletion of embryonic microglia using the CSF1R inhibitor PLX5622 has adverse sex-specific effects on mice, including accelerated weight gain, hyperactivity and anxiolytic-like behaviour. Brain Behav. Immun. *73*, 682–697.

69. Miyanishi, K., Sato, A., Kihara, N., Utsunomiya, R., and Tanaka, J. (2021). Synaptic elimination by microglia and disturbed higher brain functions. Neurochem. Int. *142*, 104901.

70. Leng, F., and Edison, P. (2021). Neuroinflammation and microglial activation in Alzheimer disease: where do we go from here? Nat. Rev. Neurol. *17*, 157–172.

71. Nguyen, P.T., Dorman, L.C., Pan, S., Vainchtein, I.D., Han, R.T., Nakao-Inoue, H., Taloma, S.E., Barron, J.J., Molofsky, A.B., Kheirbek, M.A., and Molofsky, A.V. (2020). Microglial Remodeling of the Extracellular Matrix Promotes Synapse Plasticity. Cell *182*, 388–403.e15.

72. Sipe, G.O., Lowery, R.L., Tremblay, M.È., Kelly, E.A., Lamantia, C.E., and Majewska, A.K. (2016). Microglial P2Y12 is necessary for synaptic plasticity in mouse visual cortex. Nat. Commun. *7*, 10905.

73. Miyamoto, A., Wake, H., Ishikawa, A.W., Eto, K., Shibata, K., Murakoshi, H., Koizumi, S., Moorhouse, A.J., Yoshimura, Y., and Nabekura, J. (2016). Microglia contact induces synapse formation in developing somatosensory cortex. Nat. Commun. *7*, 12540.

74. Parkhurst, C.N., Yang, G., Ninan, I., Savas, J.N., Yates, J.R., 3rd, Lafaille, J.J., Hempstead, B.L., Littman, D.R., and Gan, W.-B. (2013). Microglia promote learning-dependent synapse formation through brain-derived neurotrophic factor. Cell *155*, 1596–1609.

75. Hashimoto, A., Kawamura, N., Tarusawa, E., Takeda, I., Aoyama, Y., Ohno, N., Inoue, M., Kagamiuchi, M., Kato, D., Matsumoto, M., et al. (2023). Microglia enable cross-modal plasticity by removing inhibitory synapses. Cell Rep. *42*, 112383.

76. Eichler, A., Kleidonas, D., Turi, Z., Fliegauf, M., Kirsch, M., Pfeifer, D., Masuda, T., Prinz, M., Lenz, M., and Vlachos, A. (2023). Microglial Cytokines Mediate Plasticity Induced by 10 Hz Repetitive Magnetic Stimulation. J. Neurosci. *43*, 3042–3060.

77. Huang, Y., Wu, J., Zhang, H., Li, Y., Wen, L., Tan, X., Cheng, K., Liu, Y., Pu, J., Liu, L., et al. (2023). The gut microbiome modulates the transformation of microglial subtypes. Mol. Psychiatry *28*, 1611–1621.

78. Thion, M.S., Low, D., Silvin, A., Chen, J., Grisel, P., Schulte-Schrepping, J., Blecher, R., Ulas, T., Squarzoni, P., Hoeffel, G., et al. (2018). Microbiome Influences Prenatal and Adult Microglia in a Sex-Specific Manner. Cell *172*, 500–516.e16.

79. De Caro, C., Leo, A., Nesci, V., Ghelardini, C., di Cesare Mannelli, L., Striano, P., Avagliano, C., Calignano, A., Mainardi, P., Constanti, A., et al. (2019). Intestinal inflammation increases convulsant activity and reduces antiepileptic drug efficacy in a mouse model of epilepsy. Sci. Rep. *9*, 13983.

80. Kang, D.-W., Adams, J.B., Gregory, A.C., Borody, T., Chittick, L., Fasano, A., Khoruts, A., Geis, E., Maldonado, J., McDonough-Means, S., et al. (2017). Microbiota Transfer Therapy alters gut ecosystem and improves gastrointestinal and autism symptoms: an open-label study. Microbiome *5*, 10.

81. Kang, D.-W., Adams, J.B., Coleman, D.M., Pollard, E.L., Maldonado, J., McDonough-Means, S., Caporaso, J.G., and Krajmalnik-Brown, R. (2019). Long-term benefit of Microbiota Transfer Therapy on autism symptoms and gut microbiota. Sci. Rep. *9*, 5821.

82. Li, N., Chen, H., Cheng, Y., Xu, F., Ruan, G., Ying, S., Tang, W., Chen, L., Chen, M., Lv, L., et al. (2021). Fecal Microbiota Transplantation Relieves Gastrointestinal and Autism Symptoms by Improving the Gut Microbiota in an Open-Label Study. Front. Cell. Infect. Microbiol. *11*, 759435.

83. Tognini, P. (2017). Gut Microbiota: A Potential Regulator of Neurodevelopment. Front. Cell. Neurosci. *11*, 25.

84. Sherwin, E., Bordenstein, S.R., Quinn, J.L., Dinan, T.G., and Cryan, J.F. (2019). Microbiota and the social brain. Science *366*, eaar2016.

85. Mottolese, N., Coiffard, O., Ferraguto, C., Manolis, A., Ciani, E., and Pietropaolo, S. (2024). Autistic-relevant behavioral phenotypes of a mouse model of cyclin-dependent kinase-like 5 deficiency disorder. Autism Res. *17*, 1742–1759.

86. Yennawar, M., White, R.S., and Jensen, F.E. (2019). AMPA Receptor Dysregulation and Therapeutic Interventions in a Mouse Model of CDKL5 Deficiency Disorder. J. Neurosci. *39*, 4814–4828.

87. Jhang, C.-L., Huang, T.-N., Hsueh, Y.-P., and Liao, W. (2017). Mice lacking cyclin-dependent kinase-like 5 manifest autistic and ADHD-like behaviors. Hum. Mol. Genet. *26*, 3922–3934.

88. Okuda, K., Takao, K., Watanabe, A., Miyakawa, T., Mizuguchi, M., and Tanaka, T. (2018). Comprehensive behavioral analysis of the Cdkl5 knockout mice revealed significant enhancement in anxiety- and fear-related behaviors and impairment in both acquisition and long-term retention of spatial reference memory. PLoS One *13*, e0196587.

89. Wang, Y., Ullah, H., Deng, T., Ren, X., Zhao, Z., Xin, Y., and Qiu, J. (2024). Social isolation induces intestinal barrier disorder and imbalances gut microbiota in mice. Neurosci. Lett. *826*, 137714.

90. Dunphy-Doherty, F., O'Mahony, S.M., Peterson, V.L., O'Sullivan, O., Crispie, F., Cotter, P.D., Wigmore, P., King, M.V., Cryan, J.F., and Fone, K.C.F. (2018). Post-weaning social isolation of rats leads to long-term disruption of the gut microbiota-immune-brain axis. Brain Behav. Immun. *68*, 261–273.

91. Tognini, P., and Damiani, F. (2025). Fecal Microbiota Composition Analysis in CDKL5 Deficiency Disorder Mouse Models. (Zenodo). https://doi.org/10.5281/ZENODO.14756355

92. Schneider, C.A., Rasband, W.S., and Eliceiri, K.W. (2012). NIH Image to ImageJ: 25 years of image analysis. Nat. Methods *9*, 671–675.

93. Totaro, V., Lupori, L., and Pizzorusso, T. (2025). CounTastic: A MATLAB-Based Software for Cell Counting (Zenodo) https://doi.org/10.5281/ZENODO.14761357.

94. Lupori, L., Tognini, P., and Pizzorusso, T. Code for intrinsic signal imaging analysis in Lupori et al., 2021. https://doi.org/10.5281/zenodo.5776770.

95. Zeiss, C.J. (2021). Comparative Milestones in Rodent and Human Postnatal Central Nervous System Development. Toxicol. Pathol. *49*, 1368–1373.

96. Semple, B.D., Blomgren, K., Gimlin, K., Ferriero, D.M., and Noble-Haeusslein, L.J. (2013). Brain development in rodents and humans: Identifying benchmarks of maturation and vulnerability to injury across species. Prog. Neurobiol. *106–107*, 1–16.

97. Dell'Isola, G.B., Fattorusso, A., Pisani, F., Mastrangelo, M., Cordelli, D.M., Pavone, P., Parisi, P., Ferretti, A., Operto, F.F., Elia, M., et al. (2024). CDKL5 deficiency-related neurodevelopmental disorders: a multi-center cohort study in Italy. J. Neurol. *271*, 5368–5377.

98. Cornuti, S., Chen, S., Lupori, L., Finamore, F., Carli, F., Samad, M., Fenizia, S., Caldarelli, M., Damiani, F., Raimondi, F., et al. (2023). Brain histone beta-hydroxybutyrylation couples metabolism with gene expression. Cell. Mol. Life Sci. *80*, 28.

99. Le Naour, J., Montégut, L., Joseph, A., Garbin, K., Vacchelli, E., Kroemer, G., Pol, J.G., and Maiuri, M.C. (2022). Improved Swiss-rolling method for histological analyses of colon tissue. MethodsX *9*, 101630.

100. Erben, U., Loddenkemper, C., Doerfel, K., Spieckermann, S., Haller, D., Heimesaat, M.M., Zeitz, M., Siegmund, B., and Kühl, A.A. (2014). A guide to histomorphological evaluation of intestinal inflammation in mouse models. Int. J. Clin. Exp. Pathol. *7*, 4557–4576.

101. Remke, M., Groll, T., Metzler, T., Urbauer, E., Kövilein, J., Schnalzger, T., Ruland, J., Haller, D., and Steiger, K. (2024). Histomorphological scoring of murine colitis models: A practical guide for the evaluation of colitis and colitis-associated cancer. Exp. Mol. Pathol. *140*, 104938.

102. Benabbou, T.A., Karam, H.Z., and Karam, N.-E. (2019). Effect Oral Administration Ampicillin on the Ecological Balance of rat Enterococcal gut Microbiota. Curr. Microbiol. *76*, 329–337.

103. Clumeck, N., Thys, J.P., Vanhoof, R., Vanderlinden, M.P., Butzler, J.P., and Yourassowsky, E. (1978). Amoxicillin entry into human cerebrospinal fluid: comparison with ampicillin. Antimicrob. Agents Chemother. *14*, 531–532.

104. Cang, J., Kalatsky, V.A., Löwel, S., and Stryker, M.P. (2005). Optical imaging of the intrinsic signal as a measure of cortical plasticity in the mouse. Vis. Neurosci. *22*, 685–691.

105. Heimel, J.A., Hartman, R.J., Hermans, J.M., and Levelt, C.N. (2007). Screening mouse vision with intrinsic signal optical imaging. Eur. J. Neurosci. *25*, 795–804.

106. Murakami, M., Tognini, P., Liu, Y., Eckel-Mahan, K.L., Baldi, P., and Sassone-Corsi, P. (2016). Gut microbiota directs PPARγ-driven reprogramming of the liver circadian clock by nutritional challenge. EMBO Rep. *17*, 1292–1303.

107. Zhu, J.-W., Li, Y.-F., Wang, Z.-T., Jia, W.-Q., and Xu, R.-X. (2016). Toll-Like Receptor 4 Deficiency Impairs Motor Coordination. Front. Neurosci. *10*, 33.

108. Jurga, A.M., Paleczna, M., and Kuter, K.Z. (2020). Overview of General and Discriminating Markers of Differential Microglia Phenotypes. Front. Cell. Neurosci. *14*, 198.

109. Franco-Bocanegra, D.K., Gourari, Y., McAuley, C., Chatelet, D.S., Johnston, D.A., Nicoll, J.A.R., and Boche, D. (2021). Microglial morphology in Alzheimer's disease and after Aβ immunotherapy. Sci. Rep. *11*, 15955.

110. Schafer, D.P., Lehrman, E.K., Heller, C.T., and Stevens, B. (2014). An engulfment assay: a protocol to assess interactions between CNS phagocytes and neurons. J. Vis. Exp. 51482. https://doi.org/10.3791/51482.

STAR★METHODS

KEY RESOURCES TABLE

REAGENT or RESOURCE	SOURCE	IDENTIFIER
Antibodies		
Rabbit polyclonal anti-Iba1	FUJIFILM Wako Pure Chemical Corporation	Cat# 019–19741; RRID:AB_839504
Rat monoclonal anti-CD68, clone FA-11	BIO-RAD	Cat# MCA1957GA; RRID:AB_324217
Goat Anti-Rabbit IgG (H+L) Antibody, Alexa Fluor 568-conjugated	Invitrogen	Cat# A-11011; RRID:AB_143157
Goat Anti-Rat IgG (H+L) Antibody, Alexa Fluor 647-conjugated	Invitrogen	Cat# A-21247; RRID:AB_141778
Rabbit polyclonal anti-S100β	GeneTex	Cat# GTX129573; RRID:AB_2886037
Goat Anti-Rabbit IgG (H+L) Antibody, Alexa Fluor 488–conjugated	Invitrogen	Cat# A-11008; RRID:AB_143165
Biological samples		
Proximal colon samples from CDKL5 KO and WT mice	This study	N/A
Colon Swiss-Rolls from CDKL5 KO and WT mice	This study	N/A
Brain samples from CDKL5 KO and WT mice	This study	N/A
Fecal samples from CDKL5 KO and WT mice	This study	N/A
Chemicals, peptides, and recombinant proteins		
TRIZOL Ultrapure reagent	Fisher Molecular Biology	Cat# FS-881
Chloroform	Sigma-Aldrich	Cat# C2432
Isopropanol	PanReact AppliChem	Cat# 131090.1212
Ethanol absolute pure	PanReact AppliChem	Cat# 141086.1212
PowerUP SYBR Green Master Mix	Applied Biosystems (Thermo Fisher Scientific)	Cat# A25742
Optimal Cutting Temperature (OCT)	Scigen	Cat# 4586
Harris Hematoxylin solution	PanReact AppliChem	Cat# 253949.1610
Eosin Yellowish hydroalcoholic solution 1%	PanReact AppliChem	Cat# 251301.1211
DPX mountant	BDH	Cat# 360294H
Vancomycin Hydrochloride	Duchefa Biochemie	Cat# V0155.0005
Ampicillin sodium salt	Sigma-Aldrich	Cat# A9518
Neomycin Sulfate	Gibco (Life technologies)	Cat# 21810-031
Metronidazole	Sigma-Aldrich	Cat# M3761-25G
VECTASHIELD® Antifade Mounting Medium	Vector Laboratories	Cat# H-1000
Critical commercial assays		
QuantiTect Reverse Transcription Kit	QIAGEN	Cat# 205313
QIAamp Powerfecal DNA kit	QIAGEN	Cat# 12830-50
NexteraXT Index Kit	Illumina	Cat# FC-131- 1001/FC-131-1002
Deposited data		
16S rRNA-seq data	This study and[91]	SRA:PRJNA1232169 Zenodo: https://doi.org/10.5281/zenodo.14756355

(*Continued on next page*)

Continued

REAGENT or RESOURCE	SOURCE	IDENTIFIER
Experimental models: Organisms/strains		
CDKL5 mutant mice from Pisa vivarium	Created by Prof. Cornelius Gross, EMBL Monterotondo (Roma, Italy).	Amendola et al.[39]
CDKL5 mutant mice from Berlin vivarium	Created by Prof. Vera M. Kalscheuer, Max Planck Institute for Molecular Genetics (Berlin, Germany). Details in this study.	N/A
C57BL/6J mice	Charles River Laboratories	Jax Strain #000664
Oligonucleotides		
16S Forward (341F): 5′- CCTACGGGNGGCWGCAG -3′	Applied Genomics (IGA, Udine, Italy)	N/A
16S Reverse (805R): 5′- GGACTACHVGGGTATCTAATCC -3′	Applied Genomics (IGA, Udine, Italy)	N/A
Tjp1 Forward: 5′-CCACCTCTGTCCAGCTCTTC-3′	Eurofins Genomics	N/A
Tjp1 Reverse: 5′-CACCGGAGTGATGGTTTCT-3′	Eurofins Genomics	N/A
Cldn1 Forward: 5′-TCCTTGCTGAATCTGAACA-3′	Eurofins Genomics	N/A
Cldn1 Reverse: 5′-AGCCATCCACATCTTCTG-3′	Eurofins Genomics	N/A
tff3 Forward: 5′-TCTGGCTAATGCTGTTGGTG-3′	Eurofins Genomics	N/A
tff3 Reverse: 5′-CTCCTGCAGAGGTTTGAAGC-3	Eurofins Genomics	N/A
Rn18S Forward: 5′-CGCCGCTAGAGGTGAAATTC-3′	Eurofins Genomics	N/A
Rn18S Reverse:5′-CGAACCTCCGACTTTCGTTCT-3′	Eurofins Genomics	N/A
Software and algorithms		
ImageJ (Fiji) Software	Schneider et al.[92]	N/A
IMARIS ×64 software version 7.4.2	Bitplane	N/A
GraphPad Prism 6	GraphPad Software, San Diego, CA, USA	N/A
CounTastic	This study and[93]	Zenodo: https://doi.org/10.5281/zenodo.14761458
MATLAB code for IOS Imaging experiment analysis	Lupori et al.[37] and[94]	Zenodo: https://doi.org/10.5281/zenodo.5776770
Other		
Nanodrop 2000C Spectrophotometer	ThermoFisher Scientific	N/A
TissueLyser II	QIAGEN	Cat# 85220
StepOnePlus Real-Time PCR System	Applied Biosystems	Cat# 43766009
Cryostat	Leica Biosystems	Cat# CM1860
Nikon Eclipse E600 microscope	Nikon	N/A
LSM 900 confocal microscope	ZEISS	N/A

EXPERIMENTAL MODEL AND STUDY PARTICIPANT DETAILS

Animals

All experiments were carried out in accordance with the European Directives (2010/63/EU) and were approved by the Italian Ministry of Health.

Animals in the National Research Council Pisa Vivarium were kept in rooms at 22°C with a standard 12 h light–dark cycle, and humidity 30–50%. During the light phase, a constant illumination below 40 lux from fluorescent lamps was maintained. Food (standard diet, 4RF25 GLP Certificate, Mucedola, composed of 22% crude protein, 3.5% crude oil, 4.5% crude fiber, 7% crude ash and nutritional additives) and water were available *ad libitum* and changed weekly. Bedding material was polar wood granulate (Caipet bedding and solution), and nesting material were two paper towels, and cotton. The mice from Pisa Vivarium derive from the Cdkl5 null strain developed in,[39] and were backcrossed into C57BL/6J over seven generations.

Male wild type (WT) mice were bred with heterozygous female mice to obtain mutant and WT littermates. Weaning was performed on postnatal day (P)21–23, and mice were individually housed.

In this study, we utilized male CDKL5-/y (CDKL5 KO) mice and their male CDKL5+/y WT littermates, which have been demonstrated to faithfully recapitulate the spectrum of symptoms associated with CDD.[85]

The mice from the Pisa Vivarium were used for all the other experimental procedures and were sourced from 25 different litters. Mice were randomly assigned to either the treatment or control groups and to ensure balanced representation, animals of each genotype within a specific litter were evenly distributed between the treatment and control groups.

Data analyses were performed by experimenters blind to the animal genotype.

The mice from the Berlin vivarium used to characterize the fecal microbiota composition were derived from a conditional mutant mouse line crossed to C57BL/6J Hprt:Cre-deleter to generate the Cdkl5 KO mice with exon 4 deletion. Heterozygous Cdkl5−/+ females were bred to wild type (WT) C57BL/6J male mice for >10 generations for establishing and maintaining the colony (manuscript in preparation). All mice were housed in a centrally controlled environment with a 12 h light and 12 h dark cycle (light on at 6 a.m.), temperature of 20–22.2 °C, and humidity of 30–50%. Bedding material was polar wood granulated (Safe Select, Safe). Nesting material were two paper towels, Sizzlenest, cocoons, eco hemps and a play tunnel. Mice were fed with chow (V1124-30, Ssniff, Germany) composed of 22% crude protein, 4.5% crude fat, 3.9% crude fiber, 6.7% crude ash, and nutritional feed additives. Food and water were routinely changed.

METHOD DETAILS

Fecal DNA extraction and 16S rRNA sequencing

To analyze the composition of the fecal microbiota of CDKL5 KO and WT littermate mice at different ages, fresh feces were collected longitudinally from the same subjects at P25, P32 and P70, snap-frozen in liquid nitrogen and stored at −80°C. The ages of P25, P32, and P70 were chosen to represent distinct and critical stages of development in mice: P25 reflects early post-weaning development, analogous to childhood in humans; P32 represents a stage of neural refinement and heightened plasticity, paralleling preadolescence in humans; and P70 corresponds to young adulthood,[95,96] reflecting the typical age range of most adult patients with CDD.[97]

Feces from the Pisa Vivarium and Berlin vivarium were collected at the same time of the day, corresponding at zeitgeber time (ZT) 3, and the mice in both facilities were single-housed from weaning.

Bacterial DNA was extracted using the QIAamp Powerfecal DNA kit (Qiagen, Cat. no. 12830-50), and its concentration was quantified by the Nanodrop 2000 C Spectrophotometer (ThermoFisher Scientific).

The 16S rRNA sequencing and analysis was performed by a service offered by Institute of Applied Genomics (IGA, Udine, Italy).

Library preparation and sequencing

Libraries were prepared by following Illumina 16S Metagenomic Sequencing Library Preparation protocol in two amplification steps: an initial 35 cycle PCR amplification using locus-specific PCR primers and a subsequent amplification that integrates relevant flowcell binding domains and unique indices (NexteraXT Index Kit, Illumina, FC-131- 1001/FC-131-1002).

Primer sequences used for amplification:

16S F (341F) 5′- CCTACGGGNGGCWGCAG -3′

16S R (805R) 5′- GGACTACHVGGGTATCTAATCC -3′

Libraries were sequenced on a MiSeq instrument (Illumina) in paired end 300-bp mode read length.

Bioinformatics analysis

Reads were de-multiplexed based on the Illumina indexing system. Where amplicon length was permissive with the respective sequencing length, 3′-ends of pairs were overlapped to generate consensus pseudo-reads, while the remainders were maintained as separated pairs. After, a clipping routine is applied to remove low-quality bases at 3′tails. Reads were then retained if they maintained a minimum length of 200 bp. Any primer sequence at 5′-ends was removed and not accounted for during the process.

Following the QIIME pipelines, the USEARCH algorithm (version 8.1.1756, 32-bit) allows the following steps: chimera filtering, grouping of replicate sequences, sorting sequences per decreasing abundance and operational taxonomic unit (OTU) identification. The OTU picking aims to group query sequences into clusters, represented by centroids. Each centroid shares a level of similarity with their member sequences.

All reads were used in the analysis if they maintain a minimum length of 200 bp after removal of primer sequence and low quality bases. Paired reads with permissive overlap at their 3′-ends were merged to single fragment and used as such to improve assignment accuracy. Reads that did not support overlap were maintained in the pool for downstream processing. Sequence clustering was performed using the open-reference method with a threshold set at 97%. Sequences that passed a pre-filter step, ensuring a minimum identity of 90% with any sequence in the reference database, contributed to OTU formation. The "open-reference" analysis generated OTUs, each requiring a minimum of 2 sequenced fragments.

Rarefaction curves end-points and normalization of counts for diversity analysis are set to 50% of the target sequencing coverage (i.e., for 100,000 fragments a cutoff of 50,000 fragments is applied). The cutoff could be modified according to the sequencing yields. The total count was retained for taxonomic abundances estimation and used accordingly for ad-hoc statistical testing of taxonomic abundance when enquired.

The RDP classifier and Reference database were used to assign taxonomy with a minimum confidence threshold of 0.50. IGA Tech Reference database: 16S: modified GreenGene database (version 2013_8).

Fecal water content

Mice from the Pisa Vivarium at the beginning of their active phase (ZT 12) were placed in a clean cage without bedding, and 4–6 fecal pellets were collected immediately after evacuation. The test was performed on each mouse at P25, P32, and P42 using the same procedure. To determine fecal water content, the collected feces were weighed, dried at 100°C for 60 min, and then reweighed. The fecal water content (%) was calculated using the formula:

$$[(\text{wet weight} - \text{dry weight}) / \text{wet weight}] \times 100\%$$

Defecation frequency test and whole gut transit time measurement

Mice from the Pisa Vivarium were fasted overnight with free access to water. To assess whole gut transit time, mice at the beginning of their active phase (ZT 12) were orally gavaged with 0.1 mL of a 5% Evans Blue (w/v) solution suspended in 5% Arabic Gum (w/v) in drinking water. Immediately after gavage, mice were placed in a clean cage without bedding and monitored every 10 min until the first blue pellet was expelled. The time to the appearance of the first blue pellet was measured in minutes and constituted the whole gut transit time. Food was reintroduced 45 min post-gavage, and fecal pellet counts began at the subsequent scheduled observation time point, continuing every 10 min for a total duration of 60 min.

RNA extraction and qPCR

Proximal colon samples were harvested and subjected to total RNA extraction using the TRIZOL Extraction Isolation method (TRIZOL Ultrapure, Fisher Molecular Biology, Cat. no. FS-881). Homogenization was performed in a TissueLyser II (QIAGEN, Cat. no. 85220), by adding 1 mL TRIZOL reagent and stainless-steel beads to ~10 mg of tissue. The RNA extraction procedure was then carried out following the manufacturer's instructions.[98] In brief, chloroform (Sigma-Aldrich, Cat. no. C2432) was added and the samples were shaken for 15 s. The samples were left at RT for 3 min and then centrifuged (12000g, 15 min, 4°C). The aqueous solution, containing RNA, was collected in a fresh tube and the RNA was precipitated by the addition of isopropanol (PanReact AppliChem, Cat. no.131090.1212). Samples were mixed, left at RT for 10 min and then centrifuged (12000g, 20 min, 4°C). Supernatant was discarded and the RNA pellet was washed twice in 75% ethanol by centrifugation (2000g, 5 min, 4°C). Supernatant was discarded and the pellet was re-suspended in RNase free water. The recovered high-quality RNA (A_{260}/A_{280} ratios ≥ 2 and $A_{260}/_{230} \geq 1.8$) was DNase-treated and retrotranscribed into cDNA using the QuantiTect Reverse Transcription Kit (QIAGEN, Cat. no. 205313), according to manufacturer's instructions. Quantitative PCR (qPCR) reactions were performed in PowerUP SYBR Green Master Mix (Applied Biosystems by Thermo Fisher Scientific, Cat. no.A25742) following manufacturer instructions, using an Applied Biosystems StepOnePlus Real-Time PCR System (Cat. No. 43766009). Specifically, mRNA expression levels of the genes encoding for *tjp1* (Forward: 5′-CCACCTCTGTC CAGCTCTTC-3'; Reverse: 5′-CACCGGAGTGATGGTTTCT-3′); *cldn1* (Forward: 5′-TCCTTGCTGAATCTGAACA-3'; Reverse: 5′-AGCCATCCACATCTTCTG-3′), and *tff3* (Forward: 5′-TCTGGCTAATGCTGTTGGTG-3'; Reverse: 5′-CTCCTGCAGAGGTTT GAAGC-3′) were assessed. PCR conditions consisted in 2 hold steps at 50° C and at 95°C respectively, followed by 40 cycles with 15 s denaturation step at 95° C, and annealing/extension at 60°C for 1 min. Changes in relative gene expression were assessed via the 2-ΔΔCT method, using the 18S rRNA expression levels (*Rn18S* gene) as reference housekeeping gene (Forward: 5′-CGCCGCTAGAGGTGAAATTC-3'; Reverse:5′-CGAACCTCCGACTTTCGTTCT-3′). All oligonucleotide primers were purchased from Eurofins Genomics.

Hematoxylin and eosin (H&E) staining

Mice from Pisa Vivarium were sacrificed, and the intestinal tract was retrieved for its entire length. Measures of i) whole intestine and ii) colon were annotated. Colon tracts (from the distal end of the cecum to the proximal end of the rectum, ~3 cm length) were collected and prepared for histology examination using the Swiss Roll technique, with some modifications to the procedure previously described by.[99] Tissues were placed in a Petri dish filled with ice-cold sterile PBS, and the surrounding fat tissue was carefully removed from the organ. The inner part of the colon was then extensively cleaned by gently flushing ice-cold PBS using a gavage needle. Once all the feces were thoroughly removed, the organ was placed in a clean Petri dish and cut open longitudinally. Approximately 2–3 mm of the proximal colon end were collected and flash-frozen for subsequent RNA extraction. The remaining colon tract was gently flattened, keeping the luminal side facing up, and then carefully rolled from the proximal end towards the distal end. The rolls were then placed into molds containing Optimal Cutting Temperature (OCT) (Scigen, Tissue Plus, Cat. No. 4586) and quickly frozen on dry ice. The embedded colon rolls were stored at - 80°C until use. Frozen sections (10 μm thick) were prepared using a Cryostat (Leica, CM1860) and air-dried for at least 30 min before hematoxylin (PanReact AppliChem, Harris Hematoxylin, Cat. no. 253949.1610) and eosin (PanReact AppliChem, Eosin Yellowish hydroalcoholic solution 1%, Cat. no. 251301.1211) staining. Specifically, sections were fixed by immersion in 95% ethanol and 70% ethanol, for 2 min each, and then washed in distilled water for 5 min. Hematoxylin was applied for 2 min and washed in running water for ~15 s. Slides were then placed in 95% ethanol for 1 min; counterstained with eosin for 1 min and dehydrated through 95% alcohol, for 5 min. DPX mountant (BDH, Cat. No. 360294H) was used to cover the stained slides. Images were acquired using a Nikon Eclipse E600 microscope (Nikon Corporation, Tokyo, Japan) at 4X and 10X magnification, with a high-resolution digital camera. A total of 9 CDKL5 KO mice and 7 WT mice were analyzed. Histopathological analysis was conducted using the software ImageJ,[92] via evaluation of the following parameters: i) villi lengths and width ii) crypt layer depth; iii) muscle thickness iv) number of clusters of infiltrating monocytes.[100,101]

Antibiotic treatment

CDKL5 KO mice and WT mice from Pisa Vivarium were treated with an antibiotic cocktail (ABX, vancomycin 0.5 g/L, ampicillin 1 g/L and neomycin 1 g/L) dissolved in drinking water from weaning (P21) to P45. The ABX was refreshed every other day. Vancomycin and neomycin are not absorbed in the GI tract. Ampicillin absorption after oral administration is largely incomplete,[102] thus excluding its possibility to reach the brain, which necessitates an intravenous administration.[103] Control WT littermates and control CDKL5 KO mice were weaned at P21 and drank regular water until P45. At the end of treatment mice were transcardially perfused.

Optical imaging of the intrinsic signal (IOS)

Surgery

Surgery for IOS imaging was performed as described in.[33] P30 CDKL5 KO and WT littermates were anesthetized with isoflurane (3% induction; 1% maintenance) and head fixed on a stereotaxic frame using ear bars. Body temperature was monitored using a heating pad and a rectal probe to maintain the animals' body at 37°C. A subcutaneous injection of lidocaine (2%) was provided to anesthetize the local area, and the eyes were protected with a dexamethasone-based ointment (Tobradex, Alcon Novartis). The scalp was removed and the skull cleaned with saline. The skin was secured to the skull using cyanoacrylate and a thin layer of cyanoacrylate was poured over the exposed skull to attach a custom-made metal ring (9 mm internal diameter) centered over the binocular visual cortex. A thin layer of clear nail polish was applied over the area to ameliorate optical access. After surgery, the animals were allowed to recover fully in a heated box and monitored to ensure the absence of any sign of discomfort. Before any other experimental procedure, mice were left to recover for at least 4 days.

Imaging and data analysis

Mice were anesthetized with isoflurane (3% induction; 1% maintenance) and chlorprothixene anesthesia (1.5 mg/kg, i.p.). Images were visualized using a custom Leica microscope (Leica Microsystems). Red light illumination was provided by 6 individually addressable LEDs (WS2812) attached to the objective (Leica Z6 APO coupled with a Leica PlanApo 2.0X 10447178) by a custom 3D-printed conical holder. Visual stimuli were generated using MATLAB Psychtoolbox and presented on a gamma-corrected 24″ monitor (C24F390FHU).

IOS imaging data analysis was performed using a custom MATLAB-based algorithm available at Zenodo.[94]

Horizontal sine-wave gratings were presented in the binocular portion of the visual field enclosed in a Gaussian envelope spanning −10 to +10 degrees of azimuth and −5 to +60 (full monitor height) degrees of altitude, with a spatial frequency of 0.03 cycles per degree, mean luminance 20 cd/m^2 and a contrast of 90%. The stimulus consisted of the abrupt contrast reversal of a grating with a temporal frequency of 4 Hz for 1 s, time-locked with a 12-bit depth acquisition camera (PCO edge 5.5) using a parallel port trigger. The interstimulus time was 13 s. Frames were acquired at 30 fps with a resolution of 540 x 640 pixels. The signal was averaged for at least 8 groups of 20 trials, stimulating the contralateral eye to the recorded visual cortex. The signal was then downsampled in time to 10 fps and in space to 270 x 320 pixels. Fluctuations of reflectance (R) for each pixel were computed as the normalized difference from the average baseline (ΔR/R). For each recording, an image representing the mean evoked response was computed by averaging frames between 0.5 and 2.5 s after stimulation. The mean image was then low-pass filtered with a 2D average square spatial filter (7 pixels). To select the binocular portion of the primary visual cortex for further analysis, a region of interest (ROI) was automatically calculated on the mean image of the response by selecting the pixels in the lowest 20% ΔR/R of the range between the maximal and minimal intensity pixel.[104] To weaken background fluctuations a manually selected polygonal region of reference (ROR) was subtracted. The ROR was placed where no clear response, blood vessel artifact or irregularities of the skull were observed.[105] Mean evoked responses were quantitatively estimated as the average intensity inside the ROI.

Fecal transplantation

11 P26-P35 CDKL5 KO mice and 12 P26-P35 WT C57BL/6J mice from Pisa Vivarium belonging to 10 litters were used as donors for this experiment. Recipient mice were P28 WT C57BL/6J conventionally raised and sourced from 6 different litters. To prepare their intestines for the engraftment of a new microbiota, the recipient mice at P21 underwent a 5-day ABX treatment with vancomycin (0.5 g/L), ampicillin (1 g/L), neomycin (1 g/L), and metronidazole (1 g/L) in their drinking water before starting the fecal transplantation. After 2 days of washout, fecal transplantation was performed through oral gavage 5 times, once/day.[37,106] To avoid stress for the oral gavage, the procedure was performed for three consecutive days, the animals rested for 2 days, and finally were subjected to the gavage for another 2 days. At the time of fecal transplantation, freshly harvested donor feces were suspended in sterile PBS and mixed with a vortex for 10 min. The suspension was filtered with a cell strainer to remove large debris and immediately used for the transplantation. Every recipient mouse received 100 μL of suspension volume. After inoculation, mice remained in their home cages for 7 days to allow engraftment of the new bacterial species. They then underwent IOS imaging surgery, followed by IOS imaging 4–5 days later, and were tested in the Y-maze arena 4–5 days after that. The animals analyzed were single-housed in different cages to avoid the cage-effect on microbiota composition.

Behavioral analysis

Hindlimb clasping

Mice were suspended by their tail for 2 min and hindlimb clasping was assessed from video recordings. A lower clasping score was assigned if the mouse maintained the corresponding hindlimb clasping position for a minimum of 8 s during the observation period.

The scoring system was adapted from.[107] Specifically, a score of 4 was assigned if both hindlimbs consistently remained fully spread from the abdomen. If one hindlimb was retracted or both hindlimbs were partially retracted toward the abdomen without touching it, a score of 3 was assigned. If both hindlimbs were retracted toward the abdomen without touching each other, a score of 2 was given. If both hindlimbs were retracted, touching the abdomen and each other in a full clasping position, a score of 1 was assigned.

Nesting behavior

Mice were placed in a clean cage with two untouched nestlet (7 cm diameter rounds of pressed cotton) in the morning. The quality of the nest was scored 24 h later by mouse genotype-blind observers. The nests were evaluated on a 5-point scale as described in.[38]

Exploratory and hyperactive behavior, Y-maze

A Y-shaped maze with three symmetrical gray solid plastic arms at a 120-degree angle (26 cm length, 10 cm width, and 15 cm height) was used to test exploratory and hyperactive behaviors. Mice were placed in the center of the maze and allowed to freely explore the maze for 8 min. The apparatus was carefully cleaned with ethanol between trials to avoid the build-up of odor traces. All sessions were video recorded (Noldus Ethovision XT) for offline blind analysis. The arm entry is defined as all four limbs within the arm. A triad is defined as a set of three arm entries, when each entry is to a different arm of the maze. The number of arm entries and the number of triads were recorded to calculate the alternation percentage (generated by dividing the number of triads by the number of possible alternations and then multiplying by 100).

Immunofluorescence analysis

Mice were anesthetized with chloral hydrate (20 ml/kg BW) and perfused via intracardiac infusion with PBS and then 4% paraformaldehyde (PFA, w/vol, dissolved in 0.1 M phosphate buffer, pH 7.4). Brains were quickly removed and post-fixed overnight in PFA at 4°C, then transferred to 30% sucrose (w/vol) solution. 45 μm coronal sections were cut on a freezing microtome (Leica) and free-floating sections were processed for immunofluorescence.

Microglia analysis

Cortical sections were incubated for 1 h in a blocking solution containing 5% BSA (w/vol) and 0.3% Triton X-100 (vol/vol) in PBS and incubated overnight at 4°C with rabbit polyclonal anti-Iba1 primary antibody (FUJIFILM Wako Pure Chemical Corporation, Cat. no.019-19741; RRID:AB_839504) diluted 1:500, and rat monoclonal anti-CD68, clone FA-11 (Bio-Rad, Cat. no. MCA1957GA; RRID:AB_324217) 1:250, in PBS with 1% BSA (w/vol) and 0.1% Triton X-100 (vol/vol).

Sections were then washed with PBS and incubated for 2h at 22°C–24°C with goat anti-rabbit IgG (H+L) Alexa Fluor 568–conjugated secondary antibody (Molecular Probes (Invitrogen), Cat. no. A-11011; RRID:AB_143157) and goat anti-rat IgG (H+L) Alexa Fluor 647–conjugated secondary antibody (Molecular Probes (Invitrogen), Cat. no. A-21247; RRID:AB_141778), which was added at a dilution of 1:500 in the same solution as the primary antibody.

Sections were washed three times with PBS and mounted on slides, then they were air-dried and coverslipped with Vectashield mounting medium (Vector Laboratories, Cat. no. H-1000). Imaging was performed on an LSM 900 confocal microscope (Zeiss, Oberkochen, Germany) using a Plan-Apochromat 63x, NA:1.4 oil objective. The area of the visual cortex was defined based on the mouse brain atlas (Paxinos and Franklin's the Mouse Brain in Stereotaxic Coordinates).

The 3D reconstruction of microglial cells was performed on Z-stacks of ~40 μm, acquired with a z-step of 0.50 μm (for a final voxel size of 0.099 × 0.099 × 0.5 μm). Images were then processed for filament and soma reconstruction using respectively the "Filaments" and "Surfaces" functions of IMARIS software (Bitplane). Between 5 and 10 cortical cells were reconstructed per mouse. The analyzed morphological features were selected based on their relevance as indicators of microglia activation: filament length, number of branching points, number of terminal points, soma area, soma volume and soma sphericity (roundness).[108,109]

The phagocytic activity of microglial cells through CD68 quantitation was assessed on Z-stacks of 19.8 μm, acquired with a z-step of 1.98 μm (for each ROI, 10 fields of view containing phagocytes were acquired). The protocol used for the surface reconstruction of microglial cells and phagocytes was adapted from.[110]

Astrocyte density analysis

Cortical sections were incubated for 2 h in a blocking solution containing 10% BSA (w/vol) and 0.3% Triton X-100 (vol/vol) in PBS and incubated overnight at 4°C with rabbit polyclonal anti-S100β primary antibody (GeneTex, Cat. no. GTX129573; RRID:AB_2886037) diluted 1:250, in PBS with 5% BSA (w/vol) and 0.15% Triton X-100 (vol/vol).

Sections were then washed with PBS and incubated for 2h at 22°C–24°C with goat anti-rabbit IgG (H+L) Alexa Fluor 488–conjugated secondary antibody (Invitrogen), Cat. no. A-11008; RRID:AB_143165), which was added at a dilution of 1:500 in the same solution as the primary antibody.

Sections were washed three times with PBS and mounted on slides, then they were air-dried and coverslipped with Vectashield mounting medium (Vector Laboratories, Cat. no. H-1000). Imaging was performed on an Leica STELLARIS 5 confocal microscope (Leica Microsystem, Wetzlar, Germany) using a dry 20x objective. The area of the visual cortex was defined based on the mouse brain atlas (Paxinos and Franklin's the Mouse Brain in Stereotaxic Coordinates).

S100b positive cell counting for astrocyte density analysis was performed using a custom MATLAB-based graphical user interface called CounTastic and available at Zenodo.[93]

QUANTIFICATION AND STATISTICAL ANALYSIS

The sample sizes were based on prior studies and are indicated in the figure legend for each panel. Whenever possible, quantification and analyses were performed blind to the experimental condition. Most statistical analyses were performed using GraphPad Prism version 7 (GraphPad Software, San Diego, CA, USA). All data are represented as the mean ± SEM unless otherwise stated. N's represent single animals unless otherwise stated. Statistical significance was defined in the figure panels as follows: $*p \leq 0.05$, $**p \leq 0.01$ and $***p \leq 0.001$.

The statistical details of the experiments can be found in each figure legend.

Gut microbiota analysis: to test whether two or more groups of samples were significantly different, PERMANOVA and principal coordinate analysis (PCoA) were calculated using the Python library scikit-bio (http://scikit-bio.org/) with, respectively, the skbio.stats.distance.permanova and skbio.stats.ordination.pcoa functions. Alpha diversity significance was calculated using Mann-Whitney statistics.

Fecal water content: Statistical difference between WT and CDKL5 KO mice was tested using unpaired parametric t test when normality and homoscedasticity assumptions were respected ((i) at P25) or using Mann-Whitney U test when the samples did not follow a normal distribution ((ii) at P32 and iii) P42).

Defecation frequency test and whole GI transit time: Statistical difference between WT and CDKL5 KO mice in the defecation frequency test was assessed comparing the two cumulative distributions using a two-sample Kolmogorov-Smirnov test. Differences in the whole GI transit time were tested using the unpaired t test.

Whole GI length, colon length and spleen weight measurement: Statistical difference between WT and CDKL5 KO whole GI length, colon length and spleen absolute weight were tested using unpaired parametric t test. Statistical difference in the spleen-to-body weight ratio (%) was evaluated using Mann-Whitney U test.

Quantitative PCR (qPCR): statistical differences between expression levels of *tff3*, *tjp1* and *cldn1* in colon samples from CDKL5 KO and WT mice were assessed via unpaired parametric t test when normality and homoscedasticity assumptions were respected ((i) *tjp1* and ii) *cldn1*, or iii) using Mann-Whitney U test when the samples did not follow a normal distribution (*tff3*).

Histopathological analysis of colon sections: differences between the parameters considered for histopathological damage evaluation were assessed via unpaired parametric t test when normality and homoscedasticity assumptions were respected (i.e., muscle width, crypts layer depth, villi length and villi width), or using Mann-Whitney U test when the samples did not follow a normal distribution (i.e., clusters of infiltrating monocytes).

IOS experiments: Differences between WT CTRL, WT ABX, KO CTRL and KO ABX groups were tested for significance using two-way ANOVA. Sidak's multiple comparisons post hoc tests were performed, to correct for multiple hypothesis testing. Differences between WT recipient mice in the fecal transplantation experiment were evaluated using unpaired parametric t test, as normality and homoscedasticity assumptions were respected.

Behavioral analysis: Differences between WT CTRL, WT ABX, KO CTRL and KO ABX groups on the Y-maze, nesting and hindlimb clasping task were tested for significance using two-way ANOVA. Sidak's multiple comparisons post hoc tests were performed to correct for multiple hypothesis testing. Differences between WT recipient mice that received fecal transplants from either CDKL5 KO or WT donor mice were evaluated using unpaired parametric t test, as normality and homoscedasticity assumptions were respected.

Immunofluorescence analysis: For the analysis of the parameters related to microglia morphology (i.e., soma area, volume and sphericity, filament length, number of branching points and dendrite terminals) statistical differences between groups were assessed using two-way ANOVA, followed by Sidak's post hoc multiple comparisons test. For the Sholl analysis, a two-way ANOVA was applied for assessing interaction effects between distance from the soma and treatment, followed by Sidak's post hoc multiple comparisons test. The statistics was performed on the number of cells analyzed per each experimental group.

For astrocyte density analysis statistical differences between groups were assessed using two-way ANOVA, followed by Sidak's post hoc multiple comparisons test.

For two group comparisons we also performed a Mann-Whitney U test on data that met the assumptions of normality and homoscedasticity to ensure consistency in the statistical results (see Table S4).